TECHNICAL MEMORANDUMS

NATIONAL ADVISORY COMMITTEE FOR AERONAUTICS

No. 620

COMBINED PITCHING AND YAWING MOTION OF AIRPLANES

By A. v. Baranoff and L. Hopf

Luftfahrtforschung, Vol. 3, No. 2
March 20, 1929
Verlag von R. Oldenbourg, München und Berlin

Washington
May, 1931

NATIONAL ADVISORY COMMITTEE FOR AERONAUTICS

TECHNICAL MEMORANDUM NO. 620

COMBINED PITCHING AND YAWING MOTION OF AIRPLANES*

By A. v. Baranoff and L. Hopf

Notation

α = angle of attack
τ = angle of yaw
} See Figure 1,

Φ = angle formed by lift and perpendicular axis,

χ = angle formed by path axis and the plane, lift-perpendicular,

φ = angle formed by path axis and horizontal plane,

μ = angle formed by y-axis and the plane, path-perpendicular,

Ω = angular velocity of lift direction about the perpendicular axis
ω = angular velocity of path direction about the perpendicular axis
} Compare formula (3.3)

ω_x = angular velocity of the wind axis coordinates about the path axis,

ω_y = angular velocity of the wind axis coordinates about the lift axis,

ω_z = angular velocity of the wind axis coordinates about axis Z,

ω_ξ = angular velocity of airplane about axis ξ,

ω_η = angular velocity of airplane about axis η,

ω_ζ = angular velocity of airplane about axis ζ,

---

*"Untersuchungen über die kombinierte Seiten- und Längsbewegung von Flugzeugen," Luftfahrtforschung, Vol. 3, No. 2, March 20, 1929, pp. 39-58. Verlag von R. Oldenbourg, München und Berlin.

v = flight speed (m/s),

t = time (s),

γ = specific air density (kg/m^3),

q = dynamic pressure (kg/m^2),

b = span (m),

s = chord (m) (t being used for time),

F = wing area (m^2),

G = gross weight,

S = propeller thrust,

J_ξ, J_η, J_ζ = principal moments of inertia ($kg/m/s^2$),

k_ξ, k_η, k_ζ = inertia radii (m),

K = rolling moment about axis ξ (mkg),

L = yawing moment about axis η (mkg),

M = pitching moment about axis ζ (mkg),

c_a = lift coefficient,

c_w = drag coefficient,

c_m = moment coefficient (moment M),

c_Q = coefficient of transverse force,

c_n = coefficient of force normal to wing chord,

The sign $\dot{}$ over a letter implies differentiation according to the time, as

$$\dot{\tau} = \frac{d\tau}{dt},$$

for example.

1. Problem

The problems of stability and controllability of airplanes center about the unsteady motion of the aircraft. Whereas the

inertia forces do not enter into elementary airplane calculations, their importance in the actual flight movements is so vital that their effect on the general development of aircraft must also be included.

This report treats the problems as follows: The beginning of the investigated motions is always a setting of the lateral controls, i.e., the rudder or the ailerons. Now, the first interesting question is how the motion would proceed if these settings were kept unchanged for some time; and particularly, what upward motion would set in, how soon, and for how long, since therein lie the dangers of yawing. Two different motions ensue with a high rate of turn and a steep down slope of flight path in both but a marked difference in angle of attack and consequently different character in the resultant aerodynamic forces: one, the "corkscrew" dive at normal α, and the other, the "spin" at high α.

2. Available Data

The study of unsteady motion was first undertaken by Reissner.* Starting with the six motion equations of the airplane he, however, confined himself to small deviations from level, steady flight. Gehlen** subsequently extended Reissner's data to cover the essential typical unsteady motions, but does not go beyond the yawing motion. His method premises on the small vibrations. Baranoff and Fuchs*** follow the same principle. They also stay with the small deviations from straight flight and disregard the pitching motion, although they do effect simpler calculation methods by division into a rolling motion and a phugoid motion. Even B. M. Jones**** adheres strictly to yawing, although he rids himself of the assumption of infinitely small deviations by applying the step-by-step method. His attack is centered about the conditions in stalled flight and on the instability at high α due to the absence of damping in roll.

*H. Reissner, "Die Seitensteuerung der Flugmaschinen," Zeitschrift für Flugtechnik und Motorluftschiffahrt, Vol. 1, 1910, pp. 101 and 107.

**K. Gehlen, "Querstabilität und Seitensteuerung von Flugmaschinen," Zeitschrift für Flugtechnik und Motorluftschiffahrt, Vol. 4, 1913, pp. 173, 186, 201 and 213.

***A. v. Baranoff and R. Fuchs, "Zur Theorie der Seitenbewegung des Flugzeugs, Zeitschrift für Flugtechnik und Motorluftschiffahrt, Vol. 18, 1927, p. 32.

****B. M. Jones and A. Trevelyan, "Step-by-Step Calculations upon the Asymmetric Movements of Stalled Aeroplanes," British A.R.C. Reports and Memoranda No. 999, 1925.

B. M. Jones and others, "The Lateral Control of Stalled Aeroplanes," British A.R.C. R&M No. 1000, 1925.

B. M. Jones, "Research of the Control of Aeroplanes," Nature, No. 3054, 1928.

3. Basic Equations of Airplane Motions

Although we adhere in general to Fuchs and Hopf's text book*, we changed the descriptive variables in many cases (See Figs. 1 and 2, where both systems are shown).

First we define a system of body axis coordinates with fuselage axis ξ, strut axis η and spar axis ζ. The path of the C.G. of the airplane and the plane $\xi - \zeta$, - definable as the plane of the wing chord - forms angle of attack α, its component in the $\xi - \zeta$ plane and the ξ axis, which is in the symmetrical plane of the aircraft, forms angle of yaw τ. The lift in the plane defined by path and path component in the plane of the chord is perpendicular to the path. Thus far we follow Fuchs and Hopf; these enumerations describe the position of the path and the aerodynamic forces relative to the aircraft.

To describe the position of the path and of the aerodynamic forces in space, that is, in the earth axis system of coordinates, Fuchs and Hopf then use the plane, path-perpendicular direction (Fig. 2); with this the lift direction forms angle μ, and its component in the plane; path-perpendicular and the perpendicular direction form angle ζ. In addition ω is the angular velocity of the path axis about the perpendicular axis. This method of representation fits the conventional method of explaining the stability theory and is otherwise quite explanatory, but it fails when path and perpendicular axis coincide, because then the plane, path-perpendicular, is no longer defined and ω loses its meaning.

But since we are vitally interested in the flight attitudes in which the path is vertically or nearly vertically downward, we effect some slightly different variables. We define a plane through the two directions, perpendicular and lift, and designate the angle of the path with this plane by χ and that of its component in this plane with the perpendicular direction $\frac{\Pi}{2} - \Phi$, (Fig. 1); then Φ is the angle between the perpendicular and the lift. The lift direction turns about the perpendicular axis at angular velocity Ω, which is identical with ω, defined above, for steady motion. This definition breaks down when lift and perpendicular coincide, that is, in straight horizontal flight. The spherical triangle (Fig. 3) formed by intersection of lift, path and perpendicular, illustrates the relations between the two systems of coordinates.

---

*R. Fuchs and L. Hopf, "Aerodynamik," published by R. C. Schmidt & Co., Berlin, 1922.

The following equations are valid:

$$\left.\begin{aligned} \sin\varphi &= \sin\Phi\ \cos\chi \\ \sin\mu &= -\frac{\sin\chi\ \sin\Phi}{\sqrt{1-\sin^2\Phi\ \cos^2\chi}} \end{aligned}\right\} \tag{3.1}$$

$$\left.\begin{aligned} \cos\Phi &= \cos\varphi\ \cos\mu \\ \tan\chi &= -\frac{\sin\mu}{\tan\varphi} \end{aligned}\right\} \tag{3.2}$$

$$\omega = \Omega - \frac{d\mu}{dt}\sin\varphi + \frac{d\chi}{dt}\cos\Phi \tag{3.3}$$

The signs are, as before: τ is positive when the path direction and the right spar form an acute angle; Φ is positive when path and upward vertical form an acute angle; χ is positive in the sense of a clockwise system of rotation about the lift axis. The moments are figured positive when acting contrary to the positive sense of rotation (the clockwise system).

The force equations are written in an x-y-z system of coordinates, in which x is the path direction and y the direction of lift (y_1 in Fuchs-Hopf). Now the rate of turn of the path is

$$\left.\begin{aligned} \omega_x &= -\frac{d\Phi}{dt}\sin\chi + \Omega\sin\Phi\cos\chi \\ \omega_y &= \Omega\cos\Phi + \frac{d\chi}{dt} \\ \omega_z &= \frac{d\Phi}{dt}\cos\chi + \Omega\sin\Phi\sin\chi \end{aligned}\right\} \tag{3.4}$$

which is followed by

$$\frac{1}{g}\frac{dv}{dt} = -\sin\Phi\cos\chi + \frac{S}{G}\cos\alpha\cos\tau - c_w\frac{qF}{G} \tag{3.5}$$

$$\frac{\omega_y v}{g} = \sin\Phi\sin\chi + \frac{S}{G}\sin\tau - c_Q\frac{qF}{G} \tag{3.6}$$

$$\frac{\omega_z v}{g} = -\cos\Phi + \frac{S}{G}\sin\alpha\cos\tau + c_a\frac{qF}{G} \tag{3.7}$$

Resolved according to the temporary derivations of the angular velocities, the moment equations read:

$$\frac{d\omega_\xi}{dt} = \frac{J_\eta - J_\zeta}{J_\xi}\,\omega_\eta\,\omega_\zeta - \frac{K}{J_\xi} \tag{3.8}$$

$$\frac{d\omega_\eta}{dt} = \frac{J_\zeta - J_\xi}{J_\eta}\,\omega_\zeta\,\omega_\xi - \frac{L}{J_\eta} \tag{3.9}$$

$$\frac{d\omega_\zeta}{dt} = \frac{J_\xi - J_\eta}{J_\zeta}\,\omega_\xi\,\omega_\eta - \frac{M}{J_\zeta} \tag{3.10}$$

Here the moments of the aerodynamic forces depend, aside from v, α and τ, on the angular velocities ω_x, ω_y and ω_z.

In addition, we now have the equations which connect ω_ξ, ω_η and ω_ζ to α, τ, Φ, χ and Ω:

$$\left.\begin{aligned}
\omega_\xi &= \omega_x \cos\alpha \cos\tau + \omega_y \sin\alpha \cos\tau - \left(\omega_z + \frac{d\alpha}{dt}\right)\sin\tau \\
\omega_\eta &= -\omega_x \sin\alpha + \omega_y \cos\alpha + \frac{d\tau}{dt} \\
\omega_\zeta &= \omega_x \cos\alpha \sin\tau + \omega_y \sin\alpha \sin\tau + \left(\omega_z + \frac{d\alpha}{dt}\right)\cos\tau
\end{aligned}\right\} \tag{3.11}$$

In the following we make a step-by-step calculation of an asymmetrical motion, and state the equations so as to give a comprehensive view of the temporary change of the individual quantities relative to the value of all variables; or, in other words, we resolve the system of equations according to the temporary differential quotients of the variables. Equations (3.5), (3.8), (3.9), and (3.10) have this form already; the others yield.

$$\Omega \sin\Phi = (\omega_\xi \cos\tau + \omega_\zeta \sin\tau)\frac{\cos\chi}{\cos\alpha} - \omega_y \cos\chi \tan\alpha + \omega_z \sin\chi \tag{3.12}$$

$$\frac{d\chi}{dt} = -\Omega\cos\Phi + \omega_y = -\Omega\cos\Phi + \frac{g}{v}\left(\sin\Phi\sin\chi + \frac{S}{G}\sin\tau - c_Q\frac{qF}{G}\right) \tag{3.13}$$

$$\frac{d\Phi}{dt} = \frac{g}{v \cos \chi}\left(c_a \frac{qF}{G} + \frac{S}{G} \sin\alpha \cos\tau - \cos\Phi\right) - \Omega \sin \Phi \tan \chi \qquad (3.14)$$

$$\frac{d\alpha}{dt} = \omega_\zeta \cos\tau - \omega_\xi \sin \tau - \\ - \frac{g}{v}\left(c_a \frac{qF}{G} + \frac{S}{G} \sin\alpha \cos \tau - \cos\Phi\right) \qquad (3.15)$$

$$\frac{d\tau}{dt} = \omega\eta - \frac{d\Phi}{dt} \sin \chi \sin \alpha + \Omega \sin \Phi \cos \chi \sin \alpha - \\ - \frac{g}{v}\left(\sin \Phi \sin \chi + \frac{S}{G} \sin \tau - c_Q \frac{qF}{G}\right) \cos \alpha \qquad (3.16)$$

The temporary attitude of the motion is expressed by the nine equations (3.5), (3.8), (3.9), (3.10), (3.12) to (3.16); the reason we have nine instead of eight equations here, is because equation (3.12) contains nothing new as compared to the others, as long as we are not interested in the turning angle. We are very much interested in quantity Ω, so its elimination is not advisable.

4. Steady Motion

To begin with, it is important to know the stages of steady motion of which an airplane is capable. Straightaway flight and flight in a town have been discussed in detail, and steady spinning likewise has been thoroughly treated recently.* Still, it is apparent that this has not exhausted by a great deal all possibilities. The problem remains numerically simple as long as the control settings, which appear in the moment equations, are assumed as unknown factors, and three of the unknown of our system of equations are given instead; then χ and v and the respective control settings may be computed from certain values of α, Ω and Φ. But the control settings are in reality given quantities and the question is whether only one or more attitudes of steady flight belong to certain control settings. Even the discussion of the spinning curves** showed the ambiguity of the solutions, which now become even more pronounced. By given control settings the airplane can execute various steady motions; when the controls are deflected, an unsteady motion sets in which tends toward one of these steady attitudes, and the entire character of the motion is contingent on this final attitude. If it is the desired attitude, there is no danger, but if it is

*Comprehensive report, Bryant and Gates, "Spinning of Aeroplanes," British A.R.C. Reports and Memoranda No. 1001, 1926.
**L. Hopf, "Flight and Tail Spin Curves," Zeitschrift für Flugtechnik und Motorluftschiffahrt, 1921; also Aachen Reports No. 2.

an undesired one - and we shall see that this is always the case except in pure yawing - the controls must be set conversely, but at what setting depends again on the final attitude.

Now in order to describe the steady attitudes, we first interpret the force equations (3.5), (3.6), and (3.7), which contain no control settings. We set $d/dt = 0$ and simply consider the case of flight without engine ($S = 0$), where we disregard angle of yaw ($\tau = 0$, $c_Q = 0$). Thus,

$$\sin \Phi \cos \chi + c_w \frac{qF}{G} = 0 \tag{4.1}$$

$$\sin \Phi \sin \chi - \frac{\Omega v}{g} \cos \Phi = 0 \tag{4.2}$$

$$\cos \Phi - c_a \frac{qF}{G} + \Omega \frac{v}{g} \sin \Phi \sin \chi = 0 \tag{4.3}$$

which, rewritten, become

$$\frac{c_a}{c_w} = - \tan \chi \left(\frac{\Omega v}{g} + \frac{g}{\Omega v} \right) \tag{4.4}$$

$$\tan \Phi = \frac{\frac{\Omega v}{g}}{\sin \chi} \tag{4.5}$$

$$\frac{qF}{G} = \frac{1 + \left(\frac{\Omega v}{g} \right)^2}{c_a} \cos \Phi \tag{4.6}$$

Figure 4 illustrates equations (4.4) and (4.5); $-\frac{\Omega v}{g}$ is the abscissa, α the ordinate; χ and Φ parameters of the curves. A definite value of c_a/c_w is assigned to each α. The dotted curves are for constant χ, the full drawn curves for constant Φ, which is always negative, because we set the propeller thrust to zero. The connection between χ, $\Omega v/g$, and Φ is singular, and ambiguous between χ, $\Omega v/g$, and α, because every c_a/c_w has two values of α. (The range of negative c_a has been omitted.)

Since Φ is negative, $\Omega v/g$ and χ must always have different signs. For plotting the curves we simply select one definite sign for $\Omega v/g$. The converse sign would merely call for a contrary sign for χ, which would not affect the curve at all. The variables $\Omega v/g$, Φ and χ depend on one single air-

plane parameter - c_a/c_w - according to equations (4.4) and (4.5). A representation with α instead of c_a/c_w would be free from any individual limitation. But equation (4.6) cannot be represented in that manner. Through it every α and $\Omega v/g$ is allotted a definite qF/G (dynamic pressure divided by wing loading), in the sense that the speed is determined for a given airplane. Equation (4.6) allows the calculation of qF/G in any case; but inasmuch as this quantity does not play a material role in the other equations, we shall not enter into it.

Disregarding the lateral wind is surely of no significance in the force equations, because it may entail large moments, but no appreciable forces. Inclusion of the propeller thrust, of course changes the individual quantities, particularly Φ in normal flight. For the dangerous attitudes with vertically downward path, with which we are primarily concerned, this effect is of no particular significance.

This brings us to the moment equations, where the problem is still more simplified. Ignoring for the time being the gyroscopic moments, the moments of the aerodynamic forces disappear. All moments of these forces depend on α, τ, and the three quantities ω_x, ω_y, and ω_z, which are bound up with those used hitherto in equation (3.8). The omission of τ excludes the equation for the yawing moment L. We always assume the rudder setting such that $\tau = 0$. Now the pitching moment M depends on α and ω_z, and the rolling moment K on α, ω_x and ω_y. The conditions now become somewhat more explanatory when we neglect the dependence of M on ω_z. For the balance of the pitching moment is defined by the static wing, and control moment alone as long as we consider a purely steady pitching moment; in this case the single variable remaining by a given control setting is angle α, that is, the control setting defines α singularly (singularly, because the gyroscopic moment is ignored). During the continued directional change in a steady bank we must add now a damping moment in the equation for the pitching moments, for it affects angle α by a certain control setting; i.e., by identical control setting, different ω_z's have in reality different angles α. This effect, however, not being very pronounced, is disregarded in first approximation.

Rudder and elevator setting thus define α and τ (= 0), so there remains the yawing moment K which, for a given α and τ, depends on $\frac{\omega_x b}{v}$ and $\frac{\omega_y b}{v}$ (b = span). The moment is influenced by $\frac{\omega_x b}{v}$, because a turn about the path axis raises the angle of attack of the downward moving side of the wing (pressure side ahead), and lowers it on the other; it is affected by $\frac{\omega_y b}{v}$, because the relative speed of air and wing is always higher on the outward

side of a turning wing than on the inward side. These effects are well known; they were first measured by Bairstow, and later by other British research workers.* The dependence of the yawing moment for a certain control setting and given $\alpha - \tau$ on the two components of the rate of rotation is linear for small ω; the figures, including those for a high rate of turn may be obtained from the English data. These were arrived at by varying the values for α, τ, $\frac{\omega_x b}{v}$ and the control setting. Thus, Figure 5 and 7** show the yawing moment plotted against $\frac{\omega_x b}{v}$ and α, according to the data on the Bristol Fighter, which is a biplane with high stagger. Figure 8 shows the effect of side slip, likewise according to measurements on a biplane; Figure 9, the yawing moments replotted from Figures 5 and 7. The effect of $\frac{\omega_y b}{v}$, also for different α values has, on account of inherent difficulties, not been so widely investigated. But even here we have some data*** available, which at least supply the value of the derived moment according to $\frac{\omega_y b}{v}$. Inasmuch as we are generally concerned with small values of $\frac{\omega_y b}{v}$, such linear dependence of the moment is usually sufficient (Fig. 6).

As concerns the very marked effect of side slips on the rolling moment (Fig. 8), it is this aspect which has been neglected the most.

In order to present the balance of the forces and moments diagrammatically, the actual variables $\frac{\omega b}{v}$ of the moment equation must be converted to $\frac{\omega v}{g}$ variables of the force equations. It becomes readily apparent that the factor $\frac{v^2}{bg}$ decides this conversion and consequently the equilibrium conditions of an airplane in a bank. Thus, when we plot the respective values, which by equal aileron setting and equal α and τ correspond

---

*S. B. Gates and L. W. Bryant, "The Spinning of Aeroplanes," British A.R.C. R&M No. 1001, 1926.

**F. B. Bradfield, "Lateral Control of Bristol Fighter at Low Speeds. Measurement of Rolling and Yawing Moments of Model Wings Due to Rolling." British A.R.C. R&M No. 787, 1921.

R. A. Frazer, A. S. Batson, and A. G. Gadd, "Experiments on a Model of a British Fighter Aeroplane (1/10 scale). Part II. Lateral Derivatives by the Forced Oscillation Method." British A.R.C. R&M No. 932, 1924.

***R. G. Harris and A. S. Hartshorn, "Lateral Force and Moments on Avro Model." British A.R.C. R&M No. 924, 1924.

to a balance of the moments into a $\omega_x \frac{b}{v}$ and a $\omega_y \frac{b}{v}$ diagram, we arrive at curves whose course may be taken from measurements, and which may depend on the shape of the airplane (warping, wing setting, etc.). In the diagram of the coordinates $\omega_x \frac{v}{g}$ and $\omega_y \frac{v}{g}$, their correct position is defined by the magnitude of the conversion factor $\frac{v^2}{gb}$.

This is illustrated in Figures 10-14, computed according to the values of Figures 5 to 8. Figure 10 is continued by reflection on both axes, since it is possible to reverse the signs of the two rotation speeds. By such a reflection, Figure 12 yields the continuation of Figure 11 and vice versa; the results are similar in Figures 13 and 14.

In order to bring the balance of the rolling moment in close agreement with the force equilibrium, the latter must be changed because

$$\omega_x = \Omega \sin \Phi \cos \chi$$

$$\omega_y = \Omega \cos \Phi$$

are of real import for the moments, and not angle Φ and χ nor the rotation speed $\Omega \frac{v}{g}$ as such.

The insertion in the force equation results in a relation between $\omega_x \frac{v}{g}$ and $\omega_y \frac{v}{g}$, which is equivalent to equations (4.4) and (4.5) (Fig. 15)

$$\frac{c_a}{c_w} \frac{\omega_x v}{g} \left[1 - \left(\frac{\omega_y v}{g}\right)^2\right] + \frac{\omega_y v}{g} \left[1 + \left(\frac{\omega_x v}{g}\right)^2\right] = 0 \qquad (4.7)$$

To reestablish the connection with Figure 4, we bear in mind that

$$\frac{\Omega v}{g} = \pm \sqrt{\frac{\left(\frac{\omega_x v}{g}\right)^2 + \left(\frac{\omega_y v}{g}\right)^2}{1 - \left(\frac{\omega_y v}{g}\right)^2}} \qquad (4.8)$$

A connection between the moment and the force equilibrium exists when

$$c = \frac{v^2}{gb}$$

assumes a definite value. We multiply the abscissa and ordinate of the moment diagram (Figs. 10-14) with c, so that the curves

for the moments intersect those of the force equilibrium (Fig. 15) (example, Fig. 16). The result is one or more correlated pairs, $\frac{\omega_x v}{g}$ and $\frac{\omega_y v}{g}$ for each α which, with equation (4.8) yield $\frac{\Omega v}{g}$ as function of α.

Figure 17 shows such curves for $c = 10$ with and without aileron setting and without side slip. The effect of side slip is slight and low α (without dihedral), but at high α a side wind from the outside acts like an aileron setting on the curve and vice versa. Assuming α defined by the elevator setting, the equilibrium conditions become apparent in Figure 17. Without aileron setting we have for each α the point $\frac{\Omega v}{g} = 0$ (α axis) on the flight curve, the point on the corresponding curve of Figure 17 representing one corkscrew dive (tight spiral) and that reflected on the α axis, the other corkscrew dive.

With ailerons set, we have, as before, α values to which three $\frac{\Omega v}{g}$ values conform, although there are regions of α where $\frac{\Omega v}{g}$ assumes one singular value. Curves II and III in Figure 17 were plotted to represent one and the same control setting. By reflection on the α axis we obtain the opposite aileron setting. It is apparent that in a curve which corresponds to the aileron setting, each α has a $\frac{\Omega v}{g}$, while in the curve, plotted in opposite direction, certain α have two $\frac{\Omega v}{g}$. These two values disappear if α is either too low or too high, because when c_a is too low, there is no reserve force left to balance the centrifugal force. The range of α at which equilibrium prevails, is contingent upon c and the amount of control moment. The smaller c is, the smaller the angles α in question; just as a small control setting makes real attitudes of equilibrium at lower α possible, because the curve with vanishing control setting must always change in the corresponding curve of Figure 17 (and its reflection, which is not shown).

The general result is: By an approximate assumption that angle α is determined only by the elevator setting and the angle of yaw by the rudder setting, and if it is permissible to disregard the gyroscopic moments, every stated aileron setting (even zero setting) produces either one or three states of equilibrium. In each case ω_x and ω_y have different signs.

One of these three states of equilibrium corresponds to straight flight for zero control setting; the two curves representing the equilibrium of the forces and the rolling moment pass through the zero point. We call this the flight curve. Its characteristic is that its contingent ω_x has a different

sign from the rotating motion induced by the control setting. This fact is well known. To put an airplane in a bank, we pull down the aileron of the wing which is to go outside, so that the wing raises; but in the flight curve at which the outside wing is raised due to the higher speed, the aileron must act against it, that is, it must be set conversely. Conformal with these considerations our diagram shows a flight curve with negative ω for a positive control setting, that is, with a rotation contrary to that produced by the control setting. A positive ω_x yields a state of balance which does not agree with the flight curve; the downward path is steeper and ω_y is negative. It becomes apparent that an aileron setting forces the airplane toward such equilibrium, away from the flight curve. We call this state of balance "corkscrew." The third state is obviously a corkscrew also, but in the converse sense.

The diagram further elucidates that by high control settings or high c values (perhaps by certain α and τ also), only the corkscrew is an attitude of balance, while the flight curve does not exist at all. This, of course, is never the case nor can it be by vanishingly slight aileron setting because then the effects of the turning speed may be computed as integrals

$$K = \frac{\omega_x b}{v} \int c_n' \, \zeta^2 \, d F - \frac{\omega_y b}{v} \int 2 \, c_n \, \zeta^2 \, d F \qquad (4.9)$$

with c = coefficient of normal force c_n' = its derivation according to α, ζ the spar coordinate beginning at the plane of symmetry. The integration is carried over the whole wing area. Making $K = 0$ results in $\frac{\omega_x}{\omega_y} = - \frac{2}{c_n'} \frac{c_n}{\tau}$ as direction of the moment curve through the zero point; according to (4.7) the curve of the force equilibrium is the direction

$$\frac{\omega_x}{\omega_y} = - \frac{c_w}{c_a},$$

and this is an absolute value, always less than $\frac{2 c_n}{c_n' \tau}$, within the practical range of α; only by very small lift

$$\frac{c_w}{c_a} > \frac{2 \, c_n}{c_n'}.$$

Thus the intersections ("corkscrews") disappear only when c_n is very small; otherwise there is always a flight curve even by exceedingly slight aileron setting. If c_n is very small, i.e., in an already steep dive, an aileron setting assumes an attitude of balance which has all the characteristics of a corkscrew but which here may be designated as "flight curve."

Now we proceed to a more general representation of the feasible states of equilibrium, whose chief interest centers in the spin. For the equilibrium of the spinning curves it is essential that: 1) the moment equilibrium about the fore and aft axis prevails without any aileron setting, provided α is large enough; this is an effect of the vanishing damping in rolling (autorotation) or of the moment (shown in Fig. 8) induced by the outward side slip; 2) angle α be forced by the gyroscopic moment about the spar axis without any elevator setting. Although these conditions are known, we have replotted them for purposes of our own.

Thus Figure 18 shows the equilibrium curves of Figure 17 without aileron setting, but for different c values (to stress the values for Φ and χ). One feature here is the convergence of all curves for an angle α below the maximum of c_a. It is the result of the practically linear dependence of the rolling moment on the variables $\frac{\omega_x b}{v}$ and $\frac{\omega_y b}{v}$. The change in scale for the moment equilibrium curves due to different c values does not therefore affect their shape. But this does not include the region of autorotation beyond the lift maximum, where the dependence of $\frac{\omega_x b}{v}$ is far from linear.

Heretofore we disregarded the equilibrium of the pitching moments. But the effect of the inertia forces becomes paramount in all but very small rotations of the airplane. If $J\xi$, $J\eta$, and $J\zeta$ represent the principal inertia moments of the aircraft about its main axes, the conventional method of construction is such that the differences $J\eta - J\xi$ and $J\eta - J\zeta$ are about of the same order, while $J\xi - J\zeta$ is, in consequence, small.* On the other hand, angular velocity $\omega\xi$ and $\omega\eta$ in steady flight are usually high in ratio to $\omega\zeta$, so that the role of the gyroscopic term is confined to equation (3.10), and may be ignored in (3.8) and (3.9). Thus it becomes apparent that the inertia effect is of prime import in the balance of the yawing moments. Omitting the longitudinal damping, the equilibrium of the pitching moment is expressed as

$$c_m \, q \, F \, s = \frac{G}{g} \, (k\xi^2 - k\eta^2) \, \omega\xi \, \omega\eta \qquad (4.10)$$

Here c_m denotes the coefficient of the whole airplane with respect to the C.G. s, the wing chord, and $k\xi$, and $k\eta$, the inertia radii. Now, unless τ is too large,

$$\omega\xi \, \omega\eta = - \, (\omega_x^2 - \omega_y^2) \, \sin\alpha \cos\alpha + \omega_x \, \omega_y \, (\cos^2\alpha - \sin^2\alpha) \qquad (4.11)$$

so that equation (4.10) may be written as

*S. B. Gates and L. W. Bryant, "The Spinning of Aeroplanes." British A.R.C. R&M No. 1001, 1926.

$$\frac{c_m}{\sin\alpha\cos\alpha} = \frac{gb}{v^2}\frac{G}{qF}\frac{k\eta^2-k\xi^2}{b\ s}\left(\frac{\omega_x v}{g}\right)^2\left\{1-\left(\frac{\omega_x}{\omega_y}\right)^2 - 2\frac{\omega_x}{\omega_y}\cot 2\alpha\right\} \quad (4.12)$$

Here we encounter a new parameter which characterizes the longitudinal moment, namely,

$$\kappa = \frac{gb}{v^2}\frac{G}{qF}\frac{k\eta^2 - k\xi^2}{b\ s} \quad (4.13)$$

Now we resolve (4.12) conformal to $\frac{\omega_x v}{g}$ so that,

$$\frac{\omega_x v}{g} = \cot 2\alpha\ \frac{\omega_y v}{g} + \sqrt{\left(\frac{\omega_y v}{g}\right)^2\frac{1}{\sin^2 2\alpha} + \frac{2\ c_m}{\kappa\ \sin 2\alpha}} \quad (4.14)$$

This form is particularly suitable for computing these quantities as functions of α by applying the relation between $\frac{\omega_x v}{g}$ and $\frac{\omega_y v}{g}$ (equation 4.7) resulting from the force equilibrium. For higher α we may disregard $\left(\frac{\omega_y v}{g}\right)^2\frac{1}{\sin^2 2\alpha}$ against $\frac{2c_m}{\kappa\ \sin 2\alpha}$, so that (4.13) becomes linear. A graphical solution of the system comprising (4.7) and (4.13) is much simpler and more comprehensive than a mathematical method.

Figure 18 shows a series of curves computed in the manner described for various κ values. As concerns the dependence of these curves on c_m, its intersection with the ordinate is defined by the root of $c_m = 0$. This value of α can be affected by the stabilizer setting, elevator setting, or the position of the C.G. But it is, as a rule, confined to the usual "flight range," that is, the region between diving ($c_a = 0$) and stalled flight ($c_{a\ max}$). (Figure 19 shows the utilized figures.)

At high α we have in first approximation (as seen from (4.8) and (4.13)):

$$\frac{\Omega v}{g} = \pm\sqrt{\frac{2\ c_m}{\kappa\ \sin^2\alpha}} \quad (4.15)$$

When approaching autorotation the term on the right has a turning point whose tangent is nearly horizontal - a circumstance which explains the practically constant behavior of $\frac{\Omega v}{g}$ for high α. By elevator setting the c_m values increase or decrease by an almost constant amount (although existing measurements are confined to low α), so that the curves in our diagram, to which the approximation (4.14) applies, shift parallel only.

The intersections of a c- and a κ-curve represent a steady state of balance. Of course, the curves in the diagram do not represent the same airplane in different attitudes. For in c and in κ we find the speed v for one certain airplane resulting from α, Φ and χ, so that the same airplane in different attitudes belongs to different c and κ.

Summing up, we have three different groups of steady states: First, the one for the flight curve; this is point $\frac{\Omega v}{g} = 0$, $c_m = 0$, in the case without aileron setting (Fig. 18). With aileron setting, the intersection with the branch (not shown in Fig. 18) of our c-curve by position $\frac{\Omega v}{g}$ corresponds to the flight curve. It may happen that no such intersection occurs, as in the case of moment equilibrium ($c_m = 0$) by relatively low α, even though an equilibrium in rolling moment exists, due to too much elevator setting or too high c values for large α.

The two reflected branches of the c-curve (Fig. 18 shows only one) further intersect by a relatively low α (near $c_m = 0$) the curve of the longitudinal equilibrium. These intersections belong to the "corkscrew." Here the path is much steeper and the rotation much more violent than the corresponding flight curve for the same aileron setting. There is a certain similarity with the generally known spin. Another surprising feature is that the corkscrew, whose $\frac{\Omega v}{g}$ has the signs corresponding to the aileron setting, denotes a curve which is contrary to the flight curve but corresponds to the sense of the aileron setting. Visualizing straightaway flight, then a sudden aileron setting, the airplane leaves the flight curve relevant to this setting and approaches the corkscrew.

As third group we finally have the points at high α and $\frac{\Omega v}{g}$. These are the spinning attitudes, whose principal characteristics are the high α in the range of autorotation and the magnitude of the gyroscopic moment. We see from Figure 18 that one rotation generally has two spinning equilibriums in one direction. According to English measurements, biplanes with zero stagger still show equilibrium at $\alpha = 40^\circ$ and 60°. In such cases the c-curves revert to greater $\frac{\Omega v}{g}$ values at high α.

Now we can see in what manner the parameters affect the states of equilibrium. Making κ small, the c- and κ-curves may be shifted so far apart that spinning equilibrium ceases to exist, although it does not yet define what this means dynamically. On the other hand, appreciating that

$$\frac{G}{qF} \frac{k_\eta^2 - k_\xi^2}{b \; s}$$

remains constant while c increases, it denotes that κ is smaller. Both curves shift to the right, but the c-curve more than the other, which indicates that an increase in c facilitates spinning.

The effect of the parameter on the corkscrew equilibrium is less pronounced. It is perhaps out of the range of practical possibilities to select κ large enough to make the corkscrew equilibrium possible.

Thus far we assumed $\tau = 0$, which can be accomplished by a rudder setting. This does not signify any material limitation at low α and in airplanes without dihedral or sweepback. But it is different at high α, where the side wind affects the rolling moment considerably. A side wind from the outside shifts the c-curves at high α toward the right, thus becoming conducive to spinning; from the inside its effect is just the contrary.

The total result so far is as follows: One stated setting of the three controls generally engenders 7 states of equilibrium, that is, 1 flight curve, 2 corkscrews, and 2 spinning equilibriums each, in both directions. To this we add, moreover, one spinning equilibrium each in both directions. At certain values for c, κ and the aileron setting, such states of equilibrium may converge in pairs or disappear.

5. Initiation of Curvilinear Flight

Figures 20 and 21 show the effect of a rudder setting by different dihedral and sweepback. The assumed values of the individual airplane constants are shown in the table. We assume in Figure 20 the absence of moments due to side wind; so the motion is a pure "wind vane motion" or Dutch roll. The rudder setting turns the airplane (ω_η), but not the flight path (ω). In a turn to the right (ω_η = negative), as assumed in Figure 20, the wind must come from the left side of the wing. If this side wind is strong enough, the direction of the force on the fin and rudder is reversed and the airplane turns back.

Table of Airplane Constants and Initial Moments

Example in figures		20	21	22	24	27	28	29
Area	(m^2)	20	28	28	28	28	28	15
Weight	(kg)	610	1500	1500	1500	1500	1680	500
Span	(m)	12	14	14	14	14	14	10.6
Principal inertia radii (m)	k_ξ	1.39	1.08	1.08	1.08	1.08	2.51	1.33
	k_η	1.77	1.40	1.40	1.40	1.40	3.41	1.59
	k_ζ	1.27	1.02	1.02	1.02	1.02	2.59	1.23
Initial moment (m/kg)	K	-	-	1378	1120	1378	1378	90
	L	-545	-600	-	-600	-	-676	-144
	M	-	-	-	-	-	1320	54.5 at t=0.95

During this periodic and damped motion the flight path remains unchanged. Secondly, a rolling motion ($\omega\xi$) is produced, because the outside wing moves faster than the one on the inside; so the airplane is first correctly laid in the intended curve, and then swings toward the other side. The lateral inclination μ follows this swinging motion, but is accompanied by a systematic positive increase, which results in side slipping (term with $\frac{g}{v}$ in equation (3.16) for $\frac{d\tau}{dt}$), and thus itself increases. This is the instability in the well-known "spiral dive."

From the aspect of the curves this motion is reminiscent of the Dutch roll (as in skating), but the centrifugal force does not enter here at all; even the rolling motion has no effect whatsoever on the number of vibrations but is merely an enforced vibration with a Dutch roll period, and its amplitude is kept low by the large damping in rolling. An estimate shows the turning speed (ω) of the order of 0.01. This is so insignificantly small as to escape notice among the other disturbances. In Figure 21 we couple a rolling moment due to side wind with the lateral swinging, and in the sense to bring the airplane into the desired curve. Such an effect can be accomplished by positive dihedral of the wings (acute angle on top side) or by reversed sweepback; in addition, it occurs when the wing has reached and exceeded its lift maximum. In Figure 21 we assumed the dihedral large enough to ensure static stability. We also note the importance of the rolling turn $\omega\xi$, the engendered lateral inclination μ, and the desired turning ω of the flight path. This turning now reacts on the Dutch roll; for due to the lateral inclination a component of the gravity appears toward that side

of the airplane which systematically raises the side wind in the positive sense. Now it is easily seen what structural measures are effective. Lowering the inertia moments naturally raises the speed of the motions. Enlarging fin and rudder raises the period of vibration of ω_η and τ, so that both do not reach their minimum until later; the effect, which is followed by a turn of the flight path, is more enduring. To be sure, the damping is greater by enlarged fin and rudder, but it does not become immediately effective.

The effect of an aileron setting may be seen from Figure 22. Here it is primarily a rolling motion ω_ξ, which soon attains a constant value due to the damping in rolling. This is, as we know, proportional to the static moment of the ailerons about the fuselage axis, and inversely proportional to the damping moment of rolling. But ω_η now and τ during the whole process have the contrary sign of the preceding examples. Thus the airplane swings first contrary to the desired curve, which is caused by the turning moment of the deflected aileron, thus tending to drive the outside wing to the rear (due to higher effective α). The side wind now comes from the inside; the airplane slips inward 1. This effect is augmented by the side slip due to the lateral inclination 3; to this is added a third, purely geometrical effect represented by the second term in formula (3.16), and which is due to the fact that the turning axis of ω_ξ and the path axis do not coincide, so that ω_ξ not only changes μ but τ as well 2.

This last effect is trifling in our example; Figure 23 shows the relative proportion of the three effects on the total change in side wind. τ and ω_η behave as in the previous examples; but the added systematic effect of the side slip (due to μ) is more persisting. Now the airplane has a tendency to swing into the curve, and in fact, soon predominates the originally contrary effect. This is the typical "spiral dive" motion again.

In a combined aileron and rudder setting the rotation of the flight path is primarily due to the aileron setting; the side wind follows the rudder more. The course resembles that of Figure 21, but the speed of rotation ω remains steadier. As shown in Figure 21, the motion is very rough, but the attitudes assumed were beyond those encountered in common practice.

The direct result of the yawing motion now is a motion in the symmetrical axis of the airplane, described by ω_ζ, φ and α, which we shall, for short, call "longitudinal or pitching motion." The interactions of a lateral motion (yaw) induced by aileron or rudder on the variables of this longitudinal motion now are as follows: The airplane is turned about its spar axis

($\dot{\omega}\zeta$) by the gyroscopic moment; air force moments do not enter unless α changes.

The flight path is curved in the vertical plane ($\dot{\varphi}$) by a disturbance of the force equilibrium in the symmetrical plane. This is exclusively due to the lateral inclination (μ) of the airplane, as a result of which only the lift component $\cos \mu$ balances the weight.

In a purely longitudinal motion, a change in (α) is expressed as the difference in rotation of airplane and flight path; with lateral motion this relation becomes modified in two respects: 1) according to our definition α is not in the symmetrical plane of the aircraft, but forms the angle between the flight path and the plane of the chord. Consequently, $\omega\zeta$ acts only with component $\cos \tau$, and $\omega\xi$ through component $\sin \tau$, but since $\sin \tau$ is always small and $\cos \tau \sim 1$, while on the other hand $\omega\xi \gg \omega\zeta$, this discrepancy is significant; 2) the component of the flight-path curvature, which affects α, now is $\dot{\varphi} \cos \mu - \omega \sin \mu$, thus embracing the horizontal flight path turn as well. An airplane which describes a steady flat bank without changing its angle of attack has likewise a rotation $\omega\zeta$, which equals the rotation $\omega \sin \mu$ about the flight path.

Here also a change in α is considered as difference in rotations of airplane and flight path. It reacts on both by affecting pitching moment (c_m) and lift (c_a). As long as we consider merely the entrant motion in a bank, the longitudinal motion connected with it is secondary; its reaction on the lateral motion itself is disregarded.

There is no disturbance of force equilibrium in the case of Figure 20, because lateral inclination and flight-path curvature are wholly inessential. Owing to this, flight path and airplane do not turn in the symmetrical plane. However, α is slightly affected if rotation $\omega\xi$ meets with material values of τ; the airplane tips inward and the wind strikes it from without. This raises the angle of attack; the effect is slight, but the lift is very much dependent on α, so as a result, we note a slight raise in the flight path.

The effect of an aileron setting is first noticed, according to Figure 22, by a slight turning of $\omega\zeta$, caused by the gyroscopic moment which by $\omega\xi$ positive and $\omega\eta$ negative, is negative - that is, nose-heavy. After about half a second, the disturbance of force equilibrium, due to lateral inclination of about 10°, becomes perceptible; since the increase in μ is rapid, almost linear, φ drops somewhat parabolically. The slight effect, caused by $\omega\xi \sin \tau$, is here toward the opposite side

of that in Figure 19. Figures 25 and 26 show the relative effects on $\dot{\alpha}$ in the different cases. As soon as the flight-path curves, α would have to increase by $\dot{\varphi} \cos \mu - \omega \cos \varphi \sin \mu$ in unit time, unless the airplane is turned. This amount is always negative, because according to $-\frac{g}{v}\left(c_a \frac{qF}{G} - \cos \varphi \cos \mu\right)$ in equation (3.15) (See also (3.2)) α must become smaller. This is now followed by a decrease in lift and more rapid downward flight-path curvature, and an upward rotation of the airplane ($\dot{\omega}\xi > 0$), due to the static stability. Both actions retard the lift decrease. The figure shows a very slow drop; after a short period the value becomes constant. The process here is the opposite to that of the horizontal controls; there the airplane is rotated and the flight path curves on account of the change in α. By stability, airplane and flight path orientate themselves under a new angle of attack. Here the flight path curves under the effect of the vertical controls, which changes the angle of attack, and the airplane is turned by the stability.

The case of Figure 21 differs primarily from the lateral control by ailerons, in the sense that ω_η and τ have different signs. For the longitudinal motion this means that angle α, due to outward side slip, increases. Moreover, the effect of the gyroscopic moment on ω_ξ is righting, not depressing as in Figure 22. The same applies to Figure 24, which depicts the combined effect of aileron and rudder. The result of the momentary raise in α in these two cases is, that the flight path first rises, then drops, if the airplane is turned. The drop is retarded about 2 seconds, then sets in naturally, because the airplane inclines sideways, and the lift no longer balances the gravity. Thus it will be seen that the rudder does not help to attain a rotation velocity ω, but that in a turn the airplane holds its flying height longer with the aid of the rudder than without it. And this effect becomes more pronounced when the airplane has a low static fore-and-aft stability.

6. Motion of Entry into a Corkscrew

Now we ask the question, how a motion, once initiated by ailerons and rudder, proceeds, if the airplane is left to itself while maintaining the control setting it was given. A state of equilibrium will eventually prevail, but which one of those discussed in section 4?

The usual stability theory for conventional airplanes does not include the flight curve with nearly horizontal path, and such a state of equilibrium is expected only by static stability resulting from a pronounced dihedral.

One may doubt that the final result of the motion in Figure 21 represents an exact flight curve. According to the calculations which do not include the longitudinal motion (Gehlen, Baranoff-Fuchs) such a position may be expected. It could be attained in this case by the stable spiral diving motion. But our figure shows this motion as being so slow that the path assumes a pronounced downward slope before this effect can become active. A return - negative $\omega\xi$ - is not possible until the side wind becomes positive (i.e., coming from the inside) or, in other words, until the effect of the side slip predominates that of the Dutch roll. However, in our example (Fig. 21), the wings are almost vertical, the marked drop in flight path commences, the side slip effect fails, the corkscrew comes into being. The motion is toward the corkscrew state of equilibrium, not that of "flight curve" of Figure 16. It may be possible to induce a slow turn toward the "flight curve" by a minute aileron setting. But as a rule, the practical importance of the static lateral stability remains doubtful.

Thus, every airplane, turned into a curve by aileron and rudder has a tendency to go into downward path with constant rotation unless the controls are reset. Now the question is whether this flight is a corkscrew or a spin.

Jones' calculations and measurements show, in conformity with the stability theory, that such a motion does occur when the flight is with a high angle of attack (exceeding $c_{a\ max}$). But he failed to differentiate between corkscrew and spinning curve. Judging by the range of his measurements, the gyroscopic moments surely could not yet have been significant, so that in all probability, it was a corkscrew dive.

In Figure 27, which shows the motion of entry into a corkscrew, the characteristics of this motion become readily apparent; $\omega\xi$ rises slowly - by small vibrations, essentially due to errors of the primitive method of calculation. This rise conforms to the gradual speed increase; the absolute value $\frac{\omega\xi b}{v}$ remains constant by the given aileron setting, hence $\omega\xi$ must rise along with v. The two angles τ and α fluctuate slightly about certain equilibrium values. By equilibrium α must be smaller than in straightaway flight, with which we began, because a tail-heavy moment must act continuously on the airplane in order to turn it in the flight path and thus maintain it in constant position to it. We recognize the fluctuations of $\dot{\alpha}$ in $\omega\zeta$, as well as the proportionality between α and $\dot{\omega}\zeta$.

The equilibrium of τ is defined by the moment of the wing about the strut axis and by the effect of fin and rudder which balance this moment. Again the aerodynamic moments are quickly

balanced; again we encounter fluctuations which are similar to τ and ω_η. This $\alpha - \omega_\zeta$ evidently is the well-known turning motion, and $\tau - \omega_\eta$ the so-called Dutch roll or wind-vane motion.

Both motions now are superposed in the corkscrew by a more important one, which appears in the curves χ, Φ and Ω, and represents the force equilibrium.

To get a rough estimate of the order of magnitude of this motion, we pick out several omissions in the equations for Ω, $\dot{\chi}$, and $\dot{\Phi}$: angles τ and α are small enough so that we can write their cosine = 1 and delete the sine in the term containing the cosine. In addition, Φ near $-\frac{\pi}{2}$ and χ is small. Thus, in first approximation, we have

$$\Omega = -\omega_\xi \tag{6.1}$$

In our example, the following equilibrium values are valid for the corkscrew

$$\frac{\omega_\xi b}{v} = 0.180, \quad c_a = 0.25, \quad c_w = 0.065, \quad \frac{G}{F} = 54 \ \frac{kg}{m^2} \quad b = 14 \text{ m}$$

so that,

$$v = 115 \ \frac{m}{sec} \quad \text{and} \quad \Omega = -1.48 \ sec^{-1}$$

assuming that $\sin \Phi_o$ and $\cos \chi_o = 1$ (index o denotes equilibrium values).

Moreover, the force equations yield

$$\cos \Phi_o = \frac{c_a \frac{qF}{g}}{\left(\frac{\Omega v}{g}\right)^2 + 1} = \frac{0.250 \times 15.3}{290 + 1} = 0.0131$$

$$(\Phi_o = -89.2^\circ; \ \sin \Phi_o = -1.00)$$

$$\sin \chi_o = \frac{\Omega v}{g} \cot \Phi_o = 17.0 \times 0.0131 = 0.222$$

$$(\chi_o = 12.9^\circ; \ \cos \chi_o = 0.975)$$

In order to find this value in Figure 18, we must remember that the c-curves, by the large aileron setting of our example, spread out even at low α, (in contrast to the case without aileron setting), and that $c = 95$. This c-curve is far to the right in

Figure 18, where with the κ curve for small α it intersects in the above computed Φ_o and χ_o values. Now we set α, τ, υ and Ω constant and apply the method of small vibrations to the equations for $\dot{\Phi}$ and $\dot{\chi}$. The result is an approximate description of the motion in Figure 27. We set $\Phi_o = \Phi + \Delta\Phi$; $\chi = \chi_o + \Delta\chi$, assume $\Delta\Phi$ and $\Delta\chi$ to be infinitely small, and obtain the linear equations

$$\frac{d\,\Delta\chi}{dt} = \left(-\omega\xi \sin\Phi_o + \frac{g}{v}\cos\Phi_o \sin\chi_o\right)\Delta\Phi + \frac{g}{v}\sin\Phi_o \cos\chi_o\,\Delta\chi \qquad (6.2)$$

$$\cos\chi_o \frac{d\,\Delta\Phi}{dt} = \left(\frac{g}{v}\sin\Phi_o + \omega\xi\cos\Phi_o \sin\chi_o\right)\Delta\Phi + \omega\xi \sin\Phi_o \cos\chi_o\,\Delta\chi \qquad (6.3)$$

In first approximation we make the terms with $\frac{g}{v}$ small in contrast to those with $\omega\xi$, so the period of one vibration becomes:

$$T = \frac{2\pi}{\omega\xi}$$

In magnitude the vibration frequency of Figure 27 agrees with $\omega\xi$, but not numerically, for we are as yet far from the state of equilibrium. The further course is characterized by slow increase in speed and rotation with correspondingly shorter vibration periods. Moreover, Figure 27 shows that this corkscrew vibration is essentially slower than the superposed wind mill and turning vibrations.

Formulas (6.2) and (6.3) yield more accurate figures for the frequency and the damping of our vibration. Our numerical example gives the logarithmic increment $\frac{g}{v}$ and the vibration period $\frac{2\pi}{\omega\xi}$.

The dotted curve in Figure 27 (beginning at $t = 9$ sec) indicates the motion when the control setting is annulled. The rotation ceases almost instantaneously due to the damping in rolling; the airplane goes into a flat corkscrew dive from which it is then quickly and easily recovered.

7. Entry and Recovery from a Spin

Forced out of its flight curve, an airplane generally goes into a corkscrew dive; it is only under very special conditions that it goes into a spin. And it is fortunately so, or the number of accidents would be decidedly higher. Figures 28 and 29* show two examples of incipient spinning; Figure 29 from level flight, and Figure 28, as beginning after about 4 seconds of the attitude shown in Figure 27. Two circumstances are essential:

1) A high α where the damping in rolling fails;
2) ω_ξ and ω_η must be high and have contrary sign, to ensure effective tail-heavy gyroscopic moment.

Both motions are initiated by elevator and rudder setting respectively, or may be induced by any other extraneous disturbance.

Such a motion toward spinning may be aggravated or retarded by various circumstances. One advantage, generally known, is that obtained by raising the maximum lift (Handley Page slotted wing); it retains the damping in rolling and the effectiveness of the ailerons up to high angles of attack; the strong increase in ω_ξ at the beginning of both diagrams, Figures 28 and 29, is effectively delayed.

The motion is further decided by the values for α and τ. Only when α remains high and the side wind from the inside is not strong, can the rapid rotation ω_ξ be kept intact, and only with large ω_η and of opposite sign of ω_ξ, is it possible to turn the airplane tail-heavy enough, so that the high α may be retained. Figures 30 to 32 show the coaction of the various effects on the τ, $\dot{\alpha}$ and $\dot{\omega}_\zeta$ values of our two examples as expressed in formulas (3.16), (3.15) and (3.10). The positive terms of the sum act on the side wind in the sense of opposing the spin (in our case). 2 is due to the fact that the airplane rotation is essentially about the fuselage axis. Φ is very small except at the inception of motion, where it is negative. As long as α remains positive, this part of τ carries the opposite sign from Ω, that is, the airplane slips inward. This is a purely kinematic effect, which in every airplane acts against spinning and is, according to Figure 30, quite intense. The lateral slip (term of sum 3) also acts toward inward side slip, but becomes more and more aimless as the path continues downward and thus falls into the plane, perpendicular-lift. An outward side slip is forced by the term of sum ω_η; to spin, the rudder must be put over considerably.

*These curves were previously published. Compare 1927 Yearbook of the W.G.L. (Wissenschaftlichen Gesellschaft für Luftfahrt) p. 148.

In connection with ω_η and τ our two examples show a different aspect. In Figure 28 the opposing effects on $\dot{\tau}$ are annulled, so that a Dutch roll on τ is not noticed; the direct result of little side wind is the greater gyroscopic moment. In Figure 29, τ assumes higher values. This has a marked intensifying effect on ω_η. On the other hand, ω_η fluctuates on account of the wind-vane motion. It does not increase as strongly as in Figure 28; the gyroscopic moment remains lower. A large fin and rudder is effective for it keeps τ low and induces the wind-vane effect even at small τ.

The reversal of ω_η from negative to positive, as it occurred in the corkscrew as result of the changed direction of the gravity in the air axis coordinates (x, y, z) is of secondary importance, because the airplane is at high α to the path with lasting effect of rotation ω_x on ω_η, while by low α the effect of ω_x on ω_η is practically nil. The effect of the "autorotation" as observed in the air flow (ω_x) enters the motion ω_η with the factor $\sin \alpha$, and is always much greater than the component $\omega_y \cos \alpha$, which predominates in the corkscrew.

The rise in gyroscopic moment as seen from Figure 32, visualizes how quickly the incipient control action becomes ineffective, and how the gyroscopic moment persists against the stabilizing direction moment and the - at times - very material damping. The most effective means to combat the spinning motion would be to lower the gyroscopic moment by different mass distribution, i.e., by lowering $J\eta - J\zeta$ and κ. Greater static stability by enlarging the elevator and stabilizer, may also act favorably.

Figure 31 shows the increase in α due to the term of sum 1, that is, of the gyroscopic moment, which is responsible for $\omega\zeta$; The kinematic effect, given by 2, may either enhance or delay τ according to the sign; an inward side slip lowers α. This effect can, as shown in Figure 32, become pronounced. The 3 term of α represents the flight-path curvature in the plane of path lift; it is almost constant. Its effect is due to the excess in lift over the weight component in the lift direction; a low wing loading increases it.

The motion after reversal of the controls is shown in Figures 28 and 29, and the corresponding curves in Figures 33 to 38. Recovery from a spin in Figure 28 takes much longer than in the corkscrew dive of Figure 27; in Figure 29, this is wholly impossible within the considered time. The effect of the control measures is slow and indirect. The effect, 3-4 seconds after reversing the controls, is seen in Figure 28; there is a marked dependence of control effect on the phase of the motion. Common to both phases is the rapid decrease in $\omega\zeta$ and the slight in-

fluence of $\omega\xi$ and $\omega\eta$. Herein lies the vital difference from the corkscrew dive, where $\omega\xi$ momentarily drops to zero when the controls are put back. The course of α and τ is at wide variance in the three examples. The effect of control reversal on τ always is quite small. In the dotted case of Figure 28, the effect is rather detrimental, because the side wind tends outward. The drop in α and $\omega\xi$ is thereby retarded more quickly and $\omega\zeta$ rises again, because there is no marked drop in gyroscopic moment.

In the other case of Figure 28, α increases enormously, regardless of the elevator reversal. This is due, according to Figure 34, to the interrupted effect of the side wind which lowers α in this phase. If the side wind had been kept low for any reason, between $t = 3$ and $t = 4$ seconds, α would increase still higher and sink more quickly when $\omega\zeta$ drops. At $t = 6$ seconds, the elevator effect is finally such that α sinks below the angle α for $c_{a\ max}$, a marked damping in rolling comes into play, and the gyroscopic moment is decelerated. Here is another danger which may make the control actions ineffective - when the phases of the individual motions are distributed differently - the flight path is accelerated as the rotation $\omega\eta$ disappears, the airplane swings from the flight path into a curve, the intense side wind (almost 60° at $t = 7$ seconds) is from the outside.

In our example, the airplane is not thrown back into a spin, because α was already low enough and we had assumed no dihedral. Here we encounter a viewpoint which is opposed to a large dihedral. In the case of Figure 29, the effect of reversing the elevator, characterized by a rapid sinking of α and $\omega\zeta$, is neutralized, in so far as $\omega\eta$ increases due to the wind vane motion and the thus increasing gyroscopic moment returns the airplane to the tail-heavy sense. The flight path is approximately a helical motion about a nonvertical axis, the airplane "catches" itself from time to time; in the course of motion the axis approaches the vertical more and more. The violent motion of the airplane is far from being a steady spinning curve, although it has the principal characterisitc - insensitiveness to aerodynamic control actions due to great inertia effects.

Lacking direct measurements, we assume in this calculation an elevator efficiency extrapolated from measurements at lower α, and it remains a moot question as to whether the effectiveness is lower than we assumed here at higher α, and whether or not marked blanketing effects appear in the airplane.

Of a certainty, all unfavorable effects are materially accentuated in a "flat spin." This is due to the blanketing effect of the lower wing on the upper, as occurs in biplanes with

zero stagger at $\alpha = 40$ to 60°.

Although we did not discuss this case numerically, it is apparent that under such conditions the gyroscopic moment must become much more pronounced and the elevator less effective, so that recovery is impossible, even if sufficient time were available. Moreover, the stability of the flat spin is decidedly higher than the steep spin* discussed here.

Conclusion

Unless we limit ourselves to small deviations from level flight, yawing and pitching motion are not affected by each other; an aileron or rudder setting is followed by a yawing and a pitching motion. Because of its complexity, the motion can be studied only numerically in individual cases.

The equations of the general unsteady airplane motion are first stated so that the individual effects on the different variables of motion become apparent. The temporary derivations of the variables then appear as functions of the variables and of the structural quantities.

By certain control settings the airplane can assume various steady attitudes. Aside from the flight curve, which without aileron and rudder setting is simply a straight path, we have corkscrews and spinning curves - the former at low (normal) angles of attack and high flying speed. They are very stable, occur easily by control setting, but can be annulled by suitable control actions. In contrast to these, are the spinning curves at high α, high rate of rotation, and moderate flight speed. In these the equilibrium is not forced by aerodynamic forces, but gyroscopic moments. The possibility of equilibrium in spinning depends on the two constants

$$c = \frac{v^2}{gb}$$

and

$$\kappa = \frac{gb}{v^2} \frac{G}{qF} \frac{k_\eta^2 - k_\zeta^2}{b \; s}$$

The smaller we keep κ for a given c by appropriate mass distribution, the less is the tendency to spinning.

* A. v. Baranoff, "The Problem of Stability in Spinning." D.V.L. (Deutsche Versuchsanstalt für Luftfahrt) Yearbook, 1929, p. 175-182.

The yawing motion prevailing by the entrant motion into a curve is discussed for various cases. The rotation velocity of the path is not very materially affected by the rudder, unless the wings have a pronounced dihedral.

The most effective means against spinning would be to lower the gyroscopic moment by other than conventional mass distribution (κ small or even negative); A large fin and rudder are also quite effective, for the side wind can be kept low. The most practical method thus far is the slotted wing, which shifts the spinning curves to much higher α than in normal flight.

The numerical examples show how dependent on certain conditions are the entry and recovery, particularly on the accidental coincidence of certain α and τ.

Notwithstanding the multiplicity of ingenious experiments, the numerical data are far from being complete. Above all, we suspect that the blanketing effects in flight, particularly in stalled flight, affect the course of motion unfavorably.

Once these effects are thoroughly known, many factors can be investigated more systematically and more in detail than was done in this report.

Translation by J. Vanier,
National Advisory Committee
for Aeronautics.

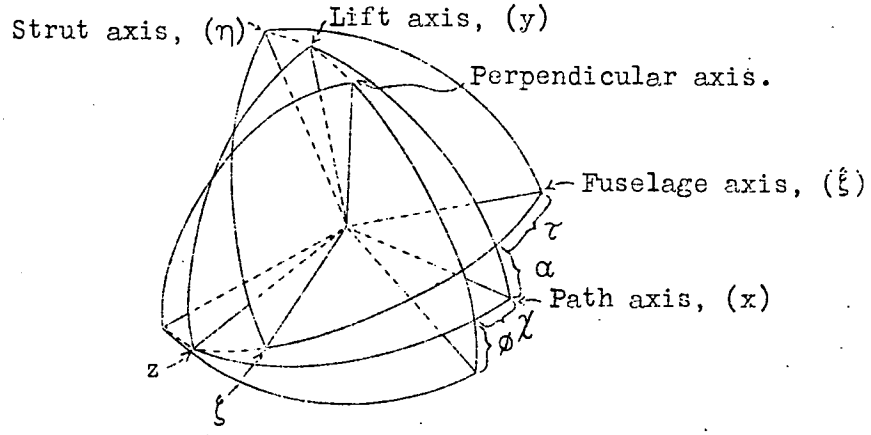

Fig. 1 I system of coordinates.

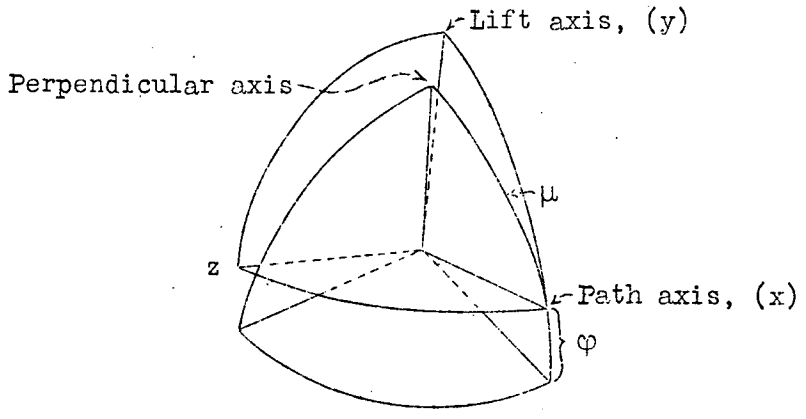

Fig. 2 II system of coordinates.

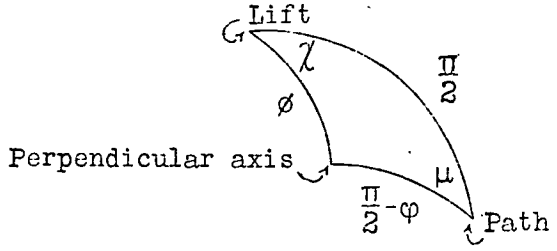

Fig. 3 Spherical triangle.

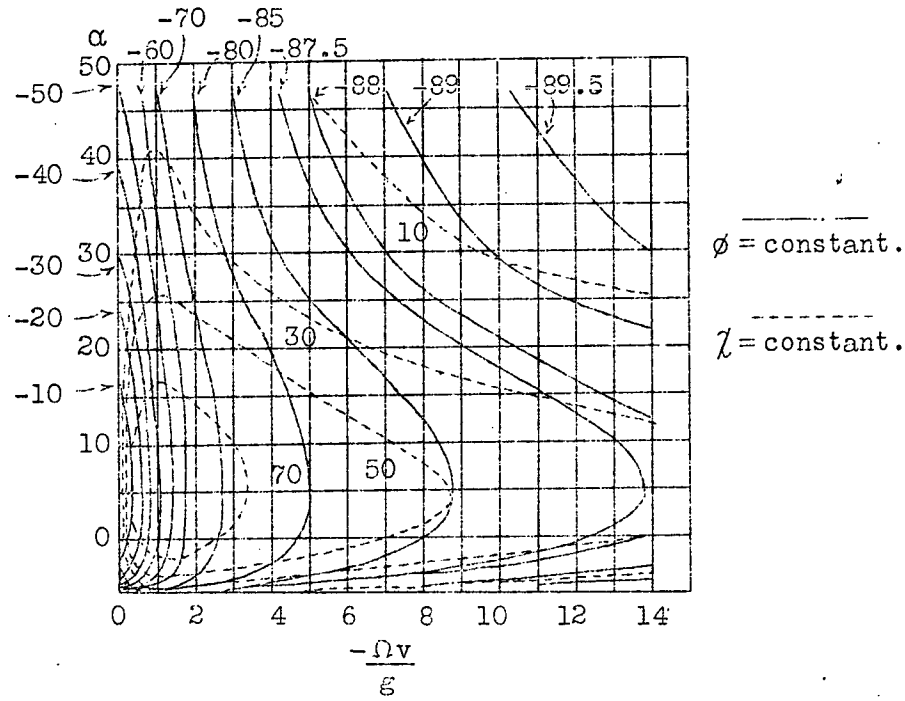

Fig. 4 $\frac{\Omega v}{g}$, α, diagram of the force equations.

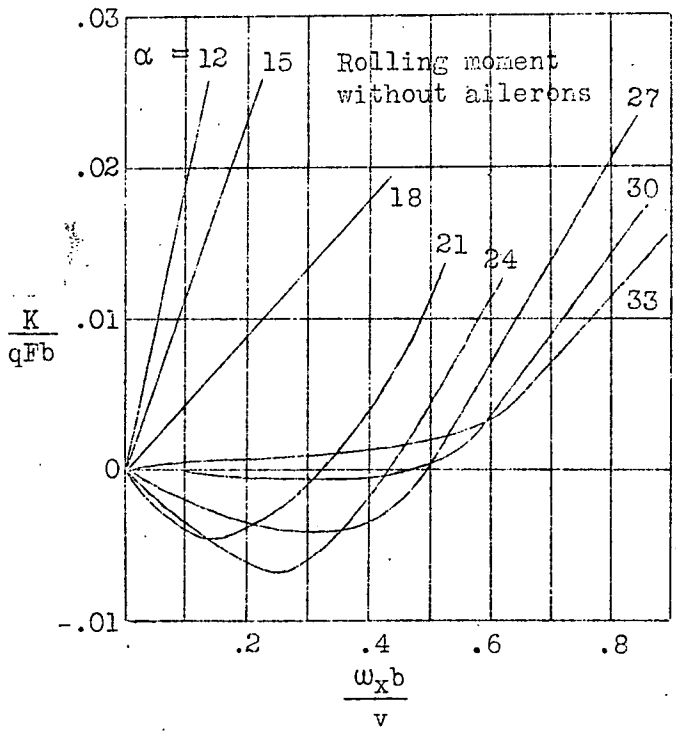

Fig. 5 Coefficient of rolling moment plotted against $\frac{\omega_x b}{v}$ without aileron setting.

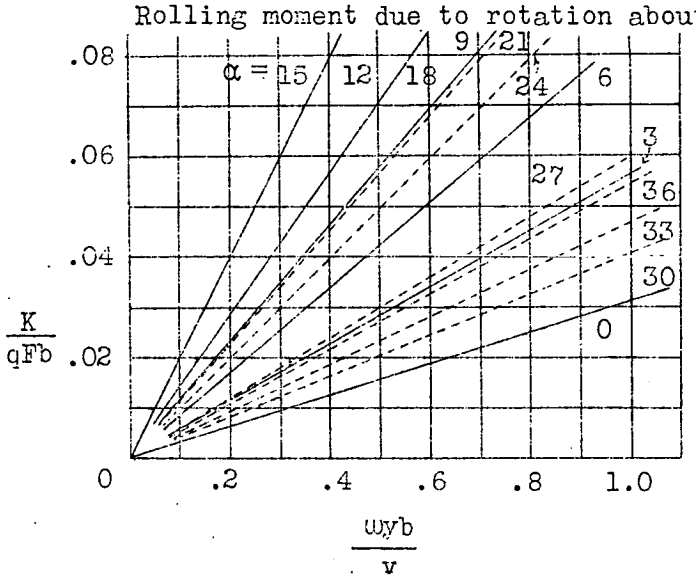

Fig. 6 Coefficient of rolling moment plotted against $\frac{\omega_y b}{v}$

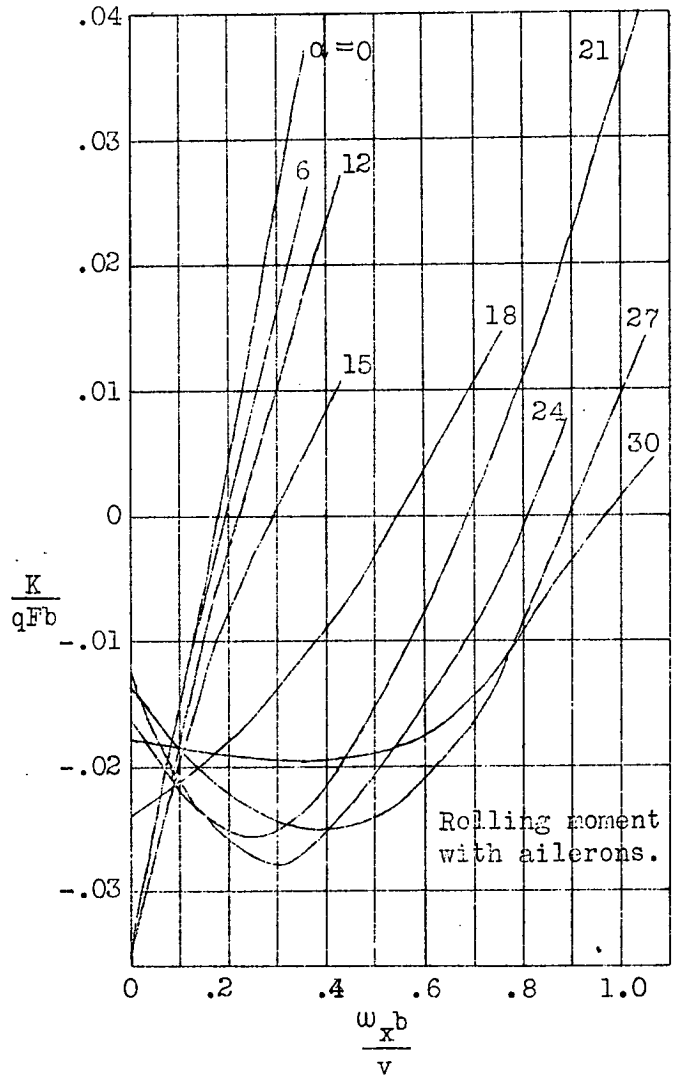

Fig. 7 Coefficient of rolling moment plotted against $\frac{\omega_x b}{v}$ with aileron setting.

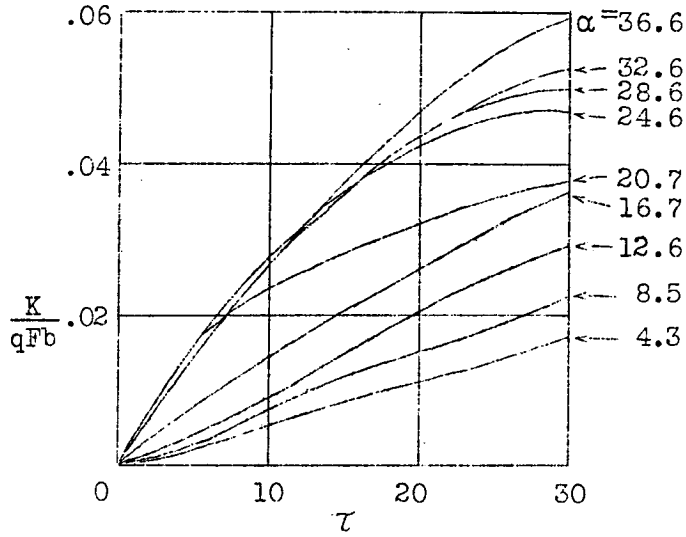

Fig. 8 Coefficient of rolling moment plotted against τ

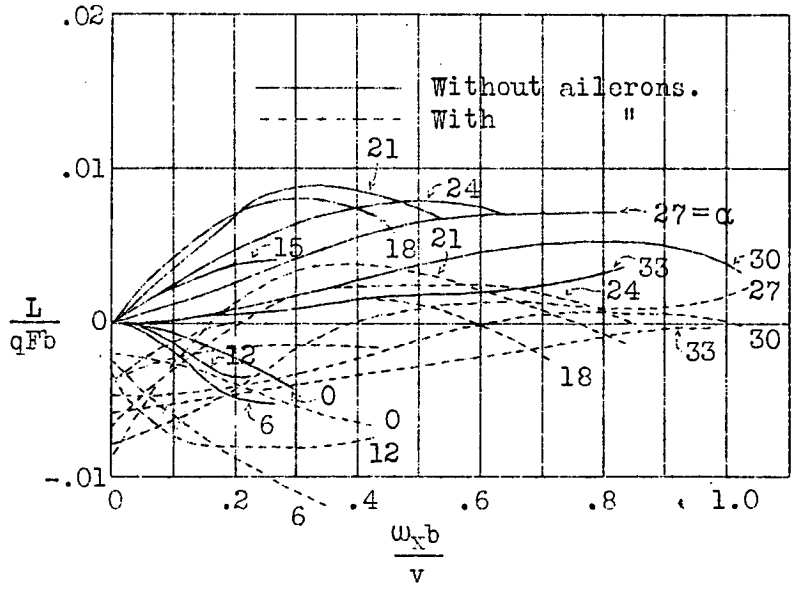

Fig. 9 Coefficient of yawing moment plotted against $\frac{\omega_x b}{v}$

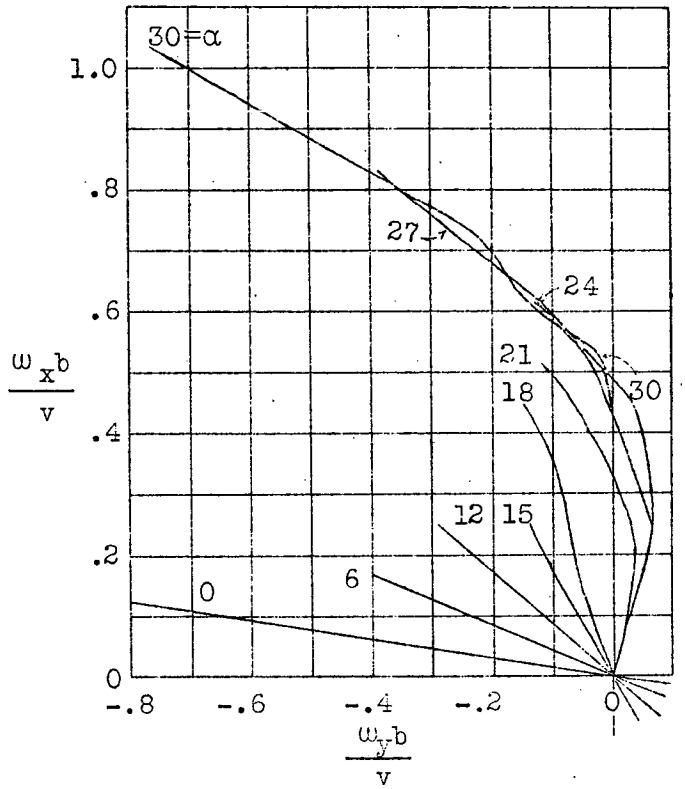

Fig. 10 Balance of rolling moment without aileron setting.

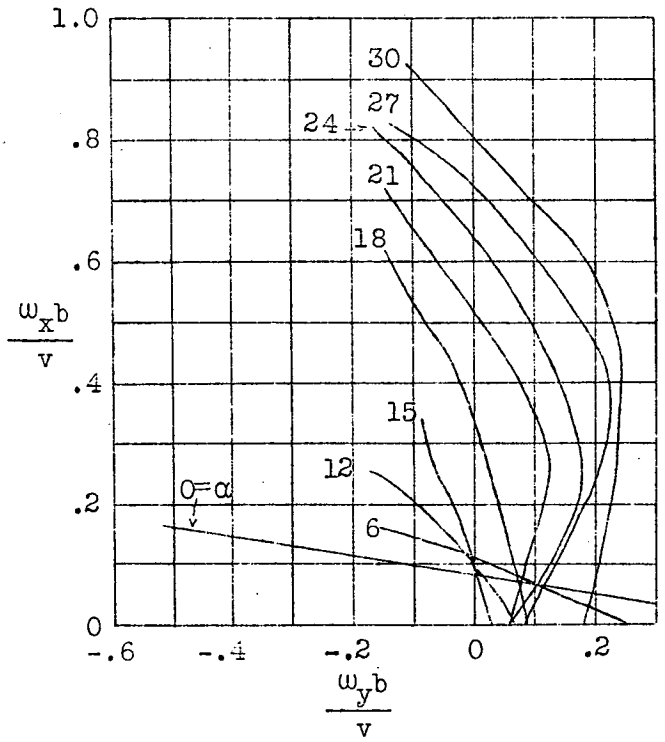

Fig. 11 Balance of rolling moment with aileron setting.

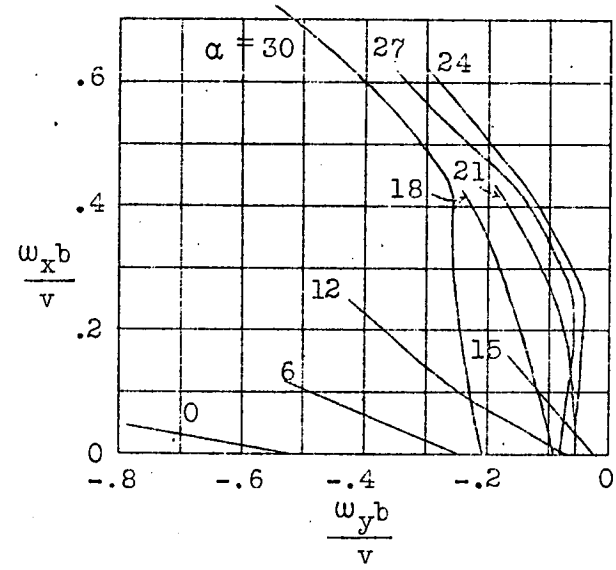

Fig. 12 Balance of rolling moment with aileron setting.(Reverse of Fig. 11)

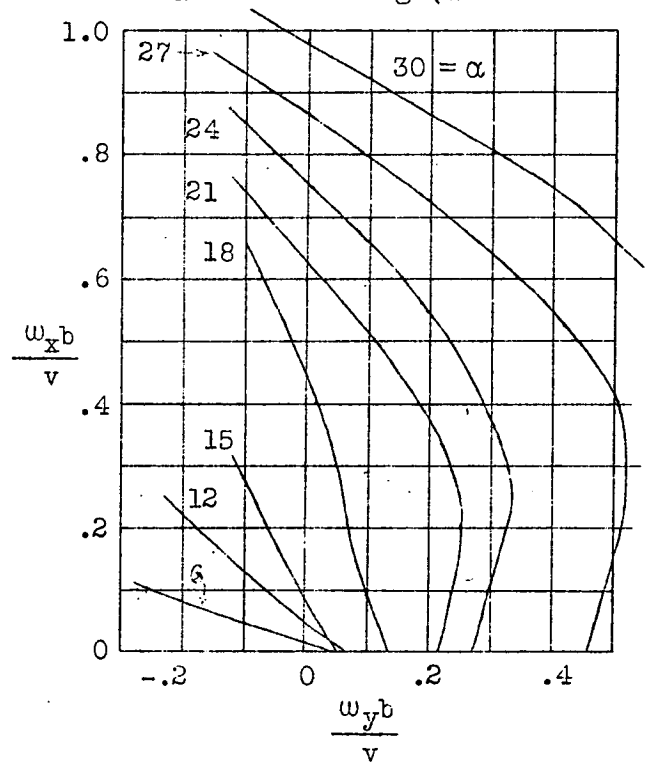

Fig. 13 Balance of rolling moment by outward sideslip.

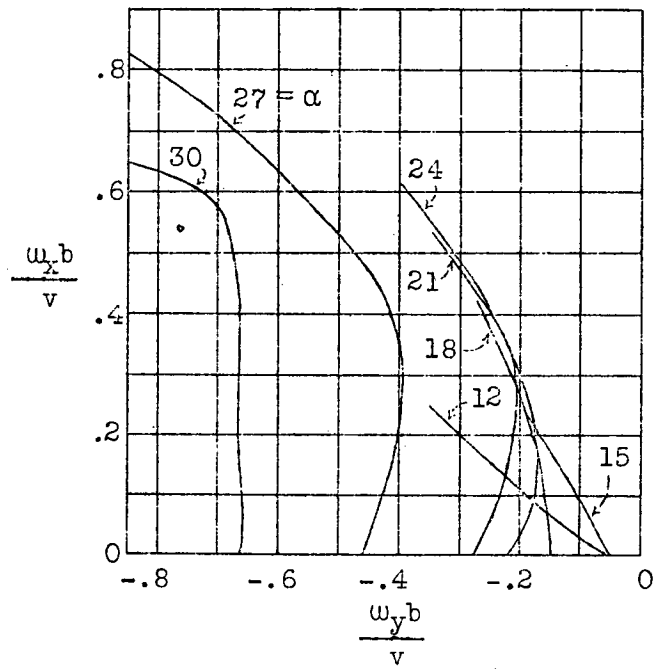

Fig. 14 Balance of rolling moment by inward sideslip.

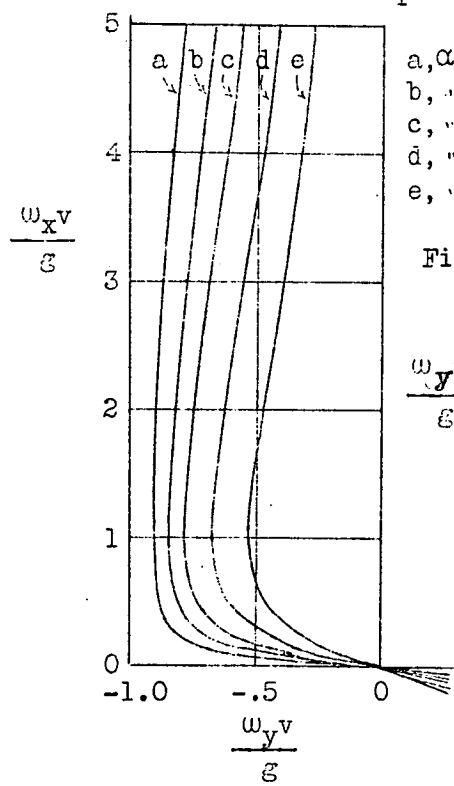

a, $\alpha = 5°$
b, " 15°, -1.3°
c, " 20°, -2.1°
d, " 25°, -4.0°
e, " 30°, -4.7°

Fig. 15 Force equilibrium in the $\frac{\omega_x v}{g}$ and $\frac{\omega_y v}{g}$ diagram.

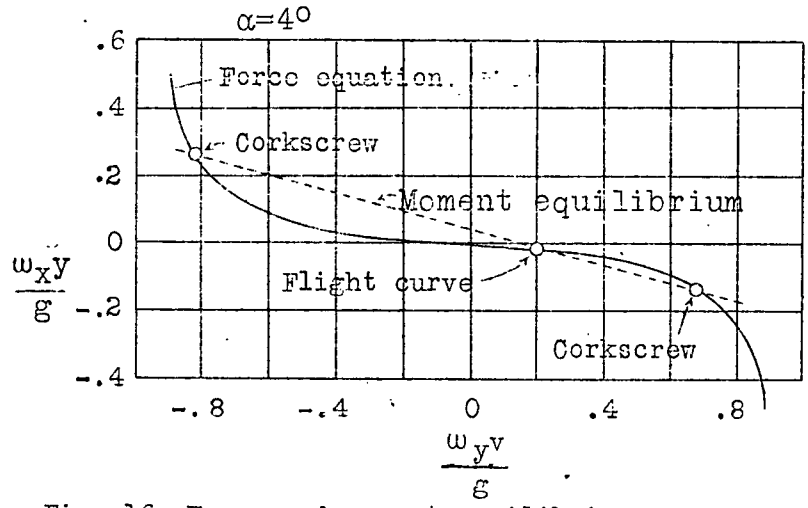

Fig. 16 Force and moment equilibrium in the $\frac{\omega_x v}{g}$ diagram and the $\frac{\omega_y v}{g}$ diagram.

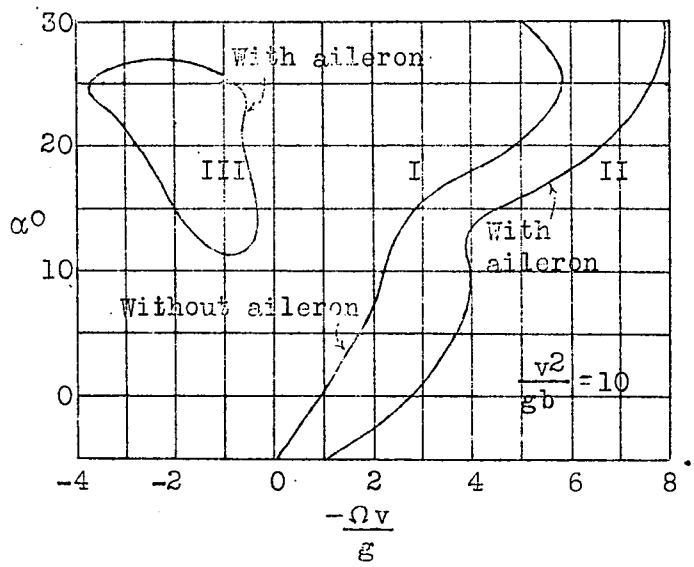

Fig. 17 Equilibrium of forces and rolling moments in $\frac{\Omega v}{g}, \alpha$, diagram.

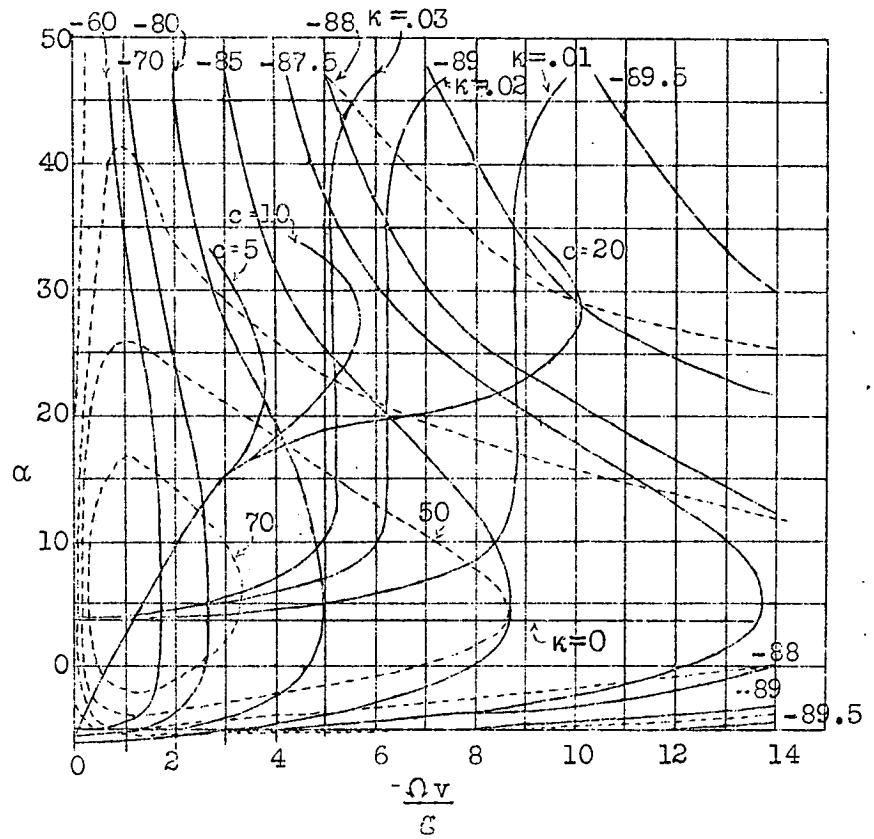

Fig. 18 Equilibrium diagram.

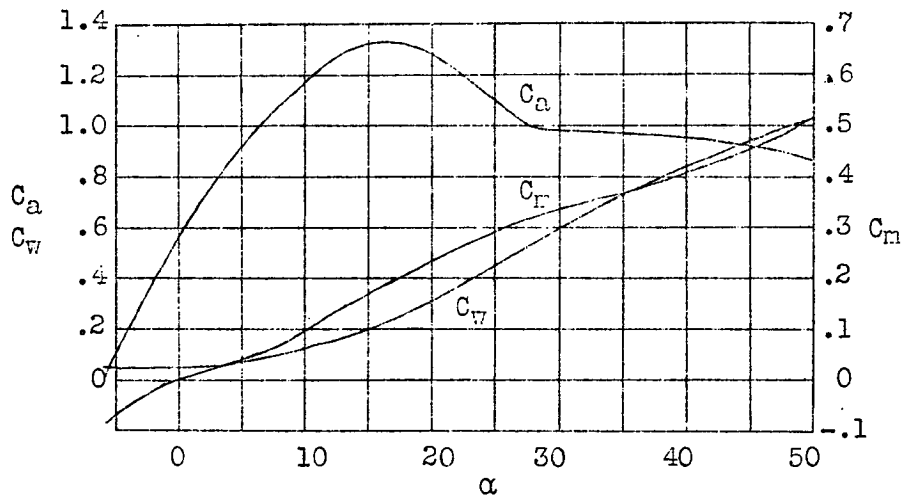

Fig. 19 C_a, C_w, and C_m values of an airplane.

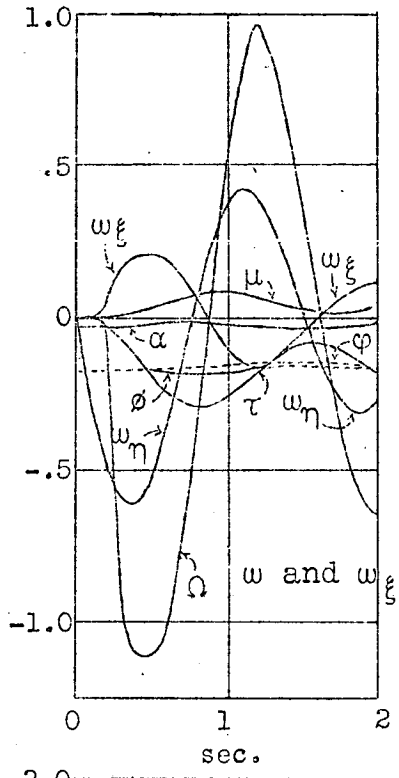

Fig. 20 Motion due to rudder setting (rolling moment independent of τ)

ω and ω_ξ practically zero.

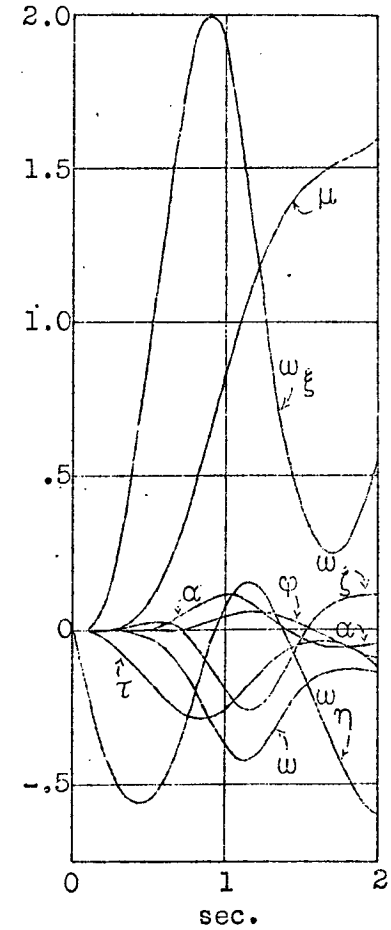

Fig. 21 Motion due to rudder setting (rolling moment dependent on τ)

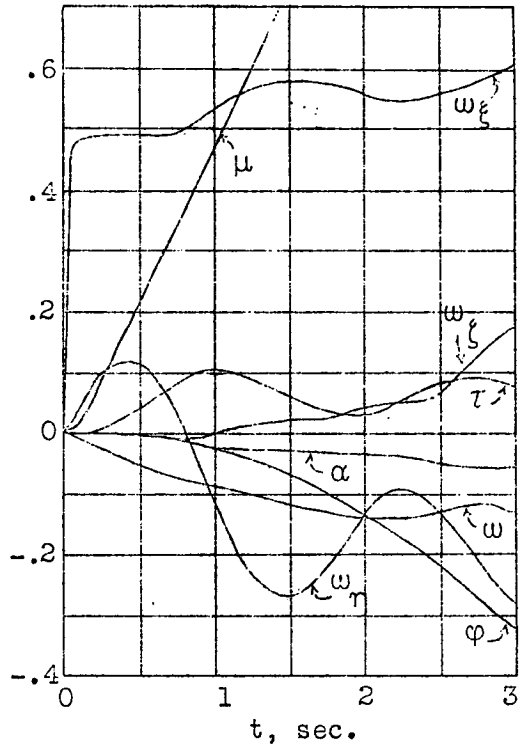

Fig. 22 Motion due to aileron setting.

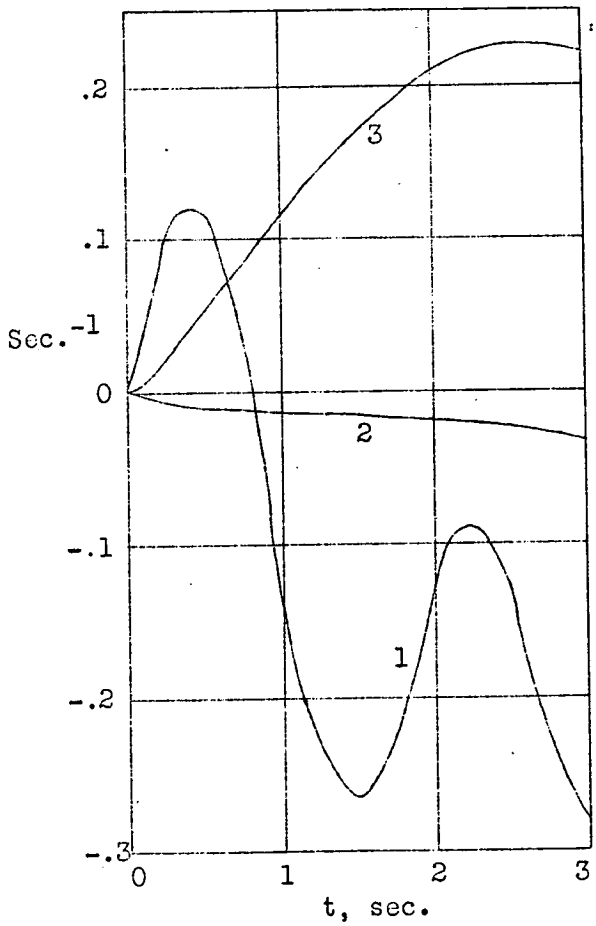

Fig. 23 Decomposition of τ for case of motion of Fig. 22

1,= ω_η

2,= $\omega_x \sin\alpha$

3,= $\frac{g}{v} \cos\varphi \sin\mu \cos\alpha$

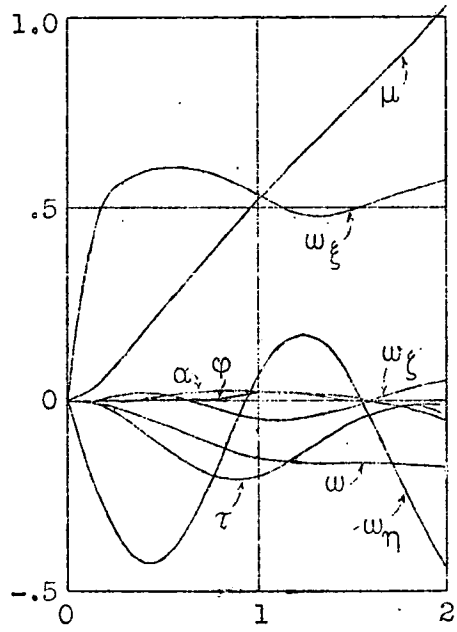

Fig. 24 Motion due to aileron and rudder setting.

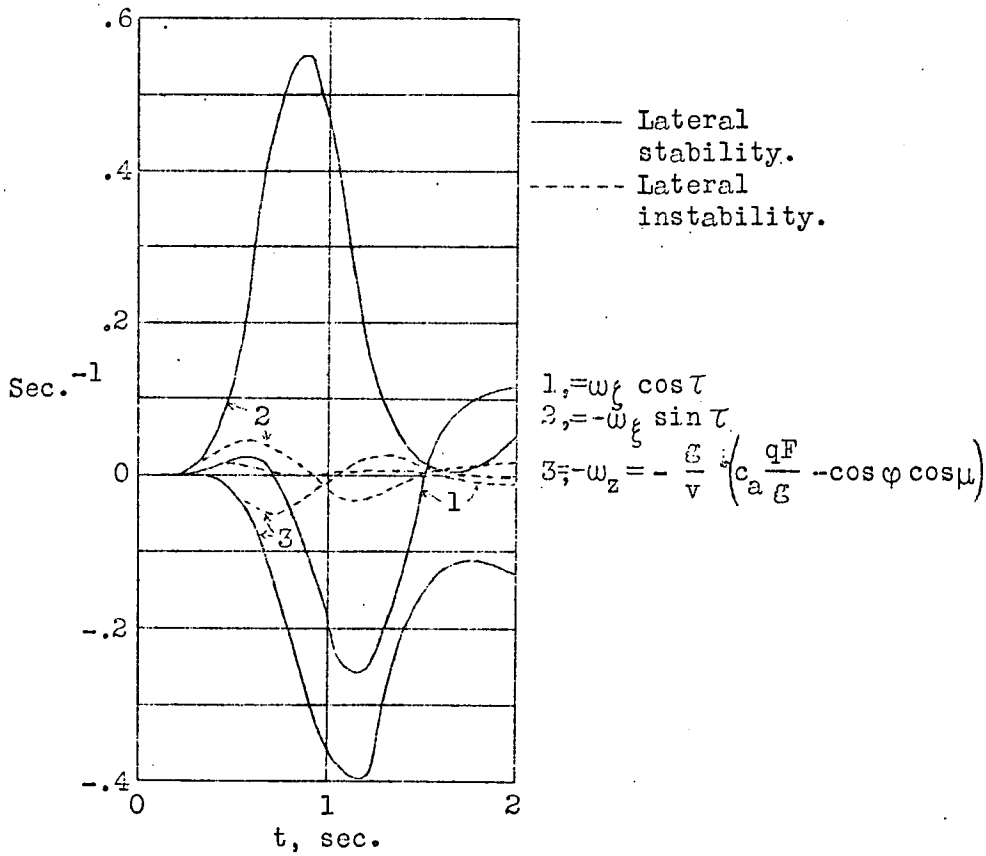

Fig. 25 Decomposition of α for case of motion of Figs. 20 and 21.

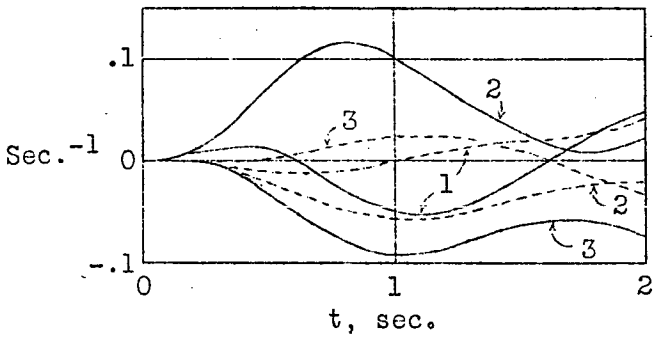

Fig. 26 Decomposition of α for case of motion of Figs. 22 and 24

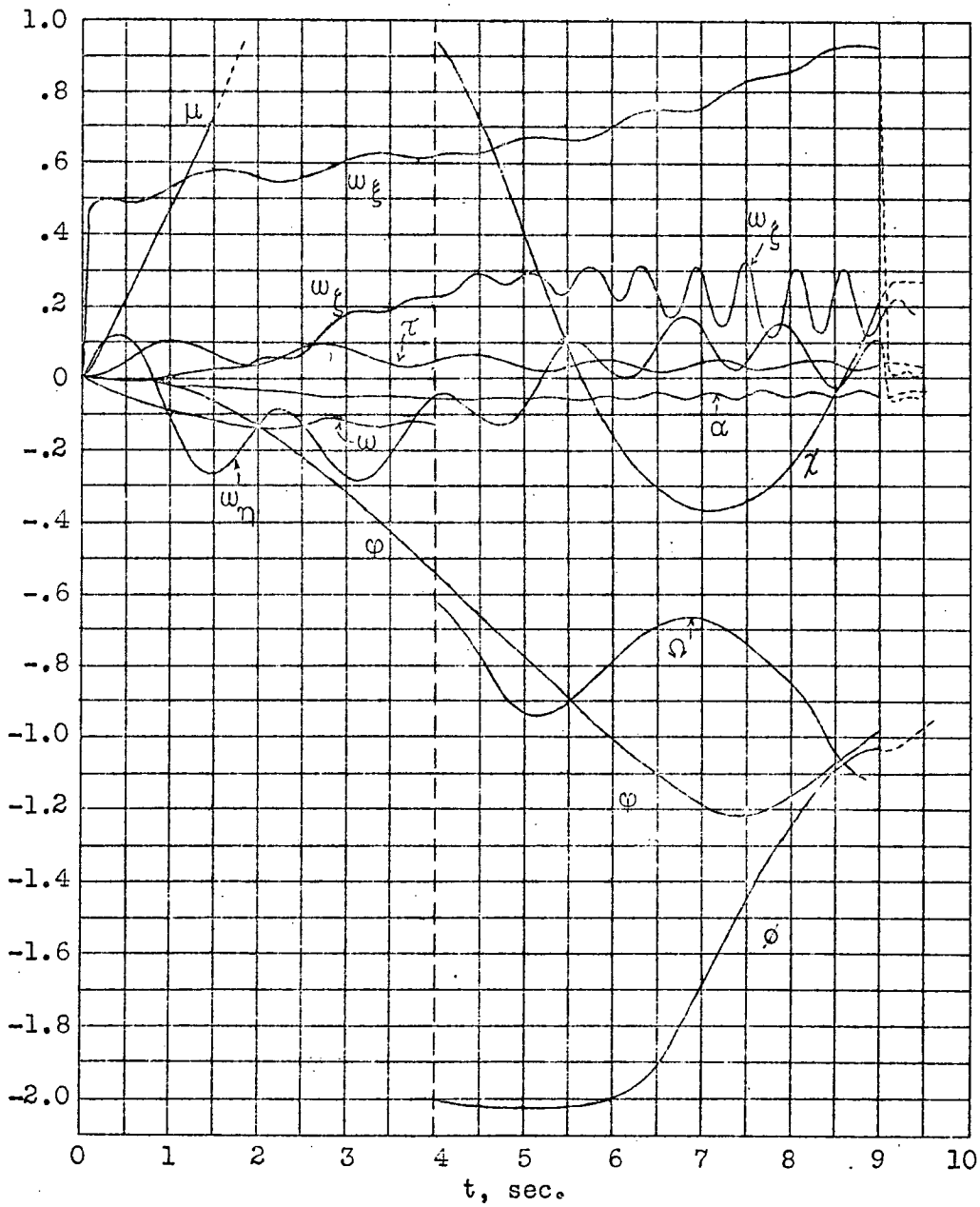

Fig. 27 Motion of entry into corkscrew.

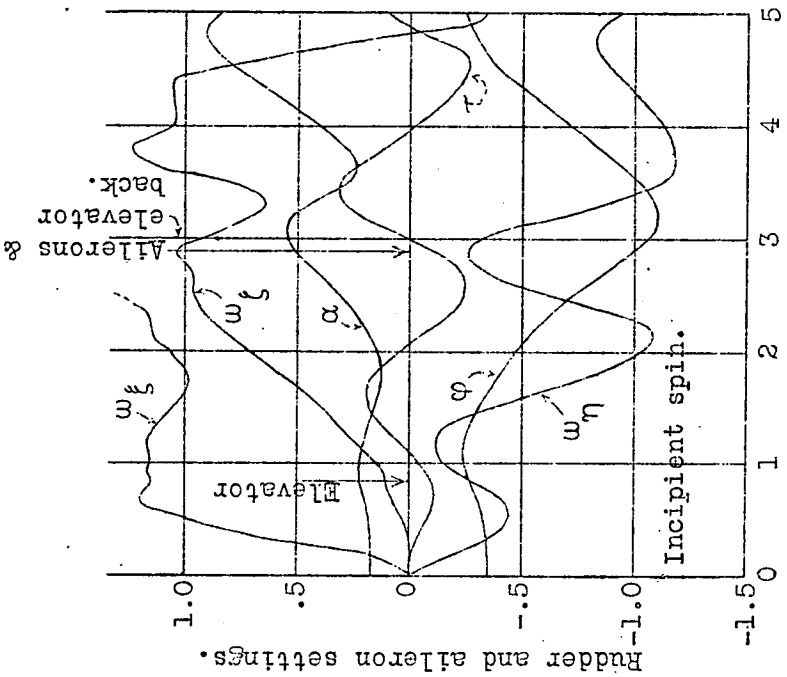

Fig. 29 Motion of entry into spin.

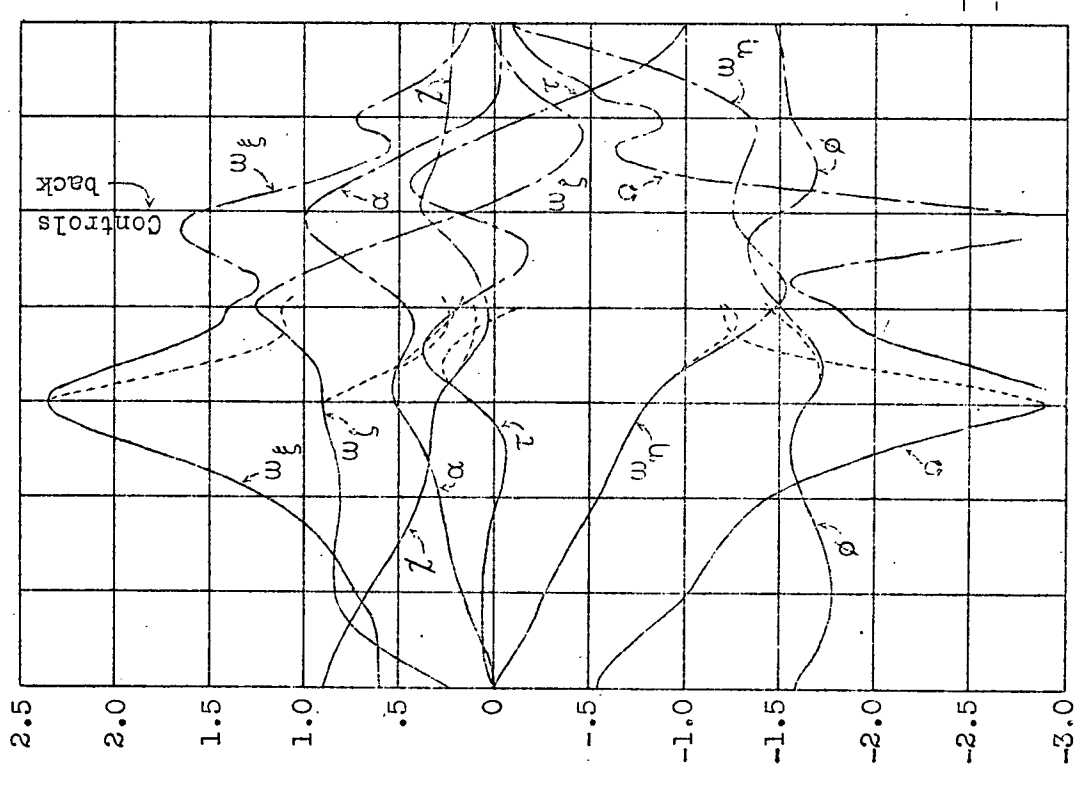

Fig. 28 Motion of entry into spin.

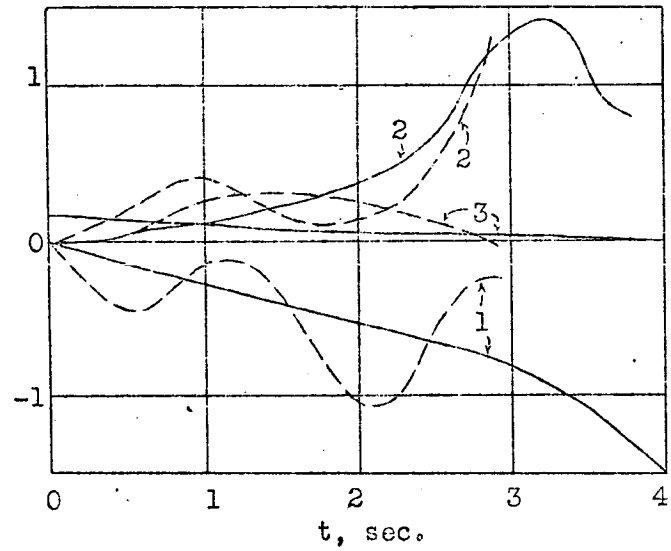

Example of Fig. 28

1,=ω_η
2,=$\omega_x \sin\alpha = (-\phi \sin\chi + \Omega \sin\phi \cos\chi)\sin\alpha$
3,=$\frac{g}{v} \sin\phi \sin\chi \cos\alpha$

Fig. 30 Decomposition of τ for case of Figs. 28 & 29.

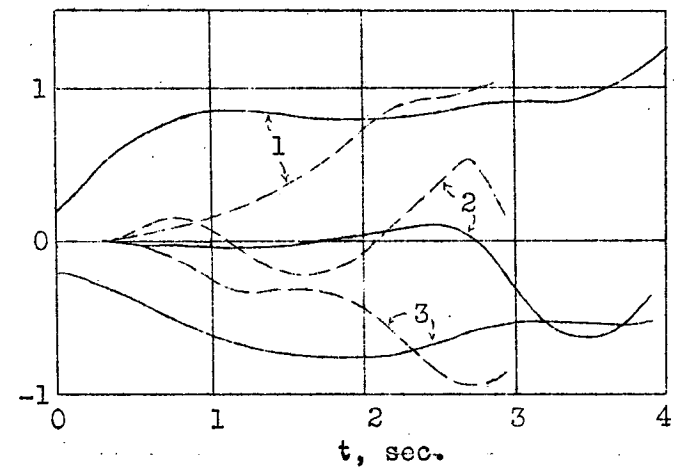

Example of Fig. 29

1,=$\omega_\zeta \cos\tau$
2,=$-\omega_\xi \sin\tau$
3,=$-\frac{g}{v}\left(c_a \frac{qF}{g} - \cos\phi\right)$

Fig. 31 Decomposition of α for case of Figs. 28 & 29.

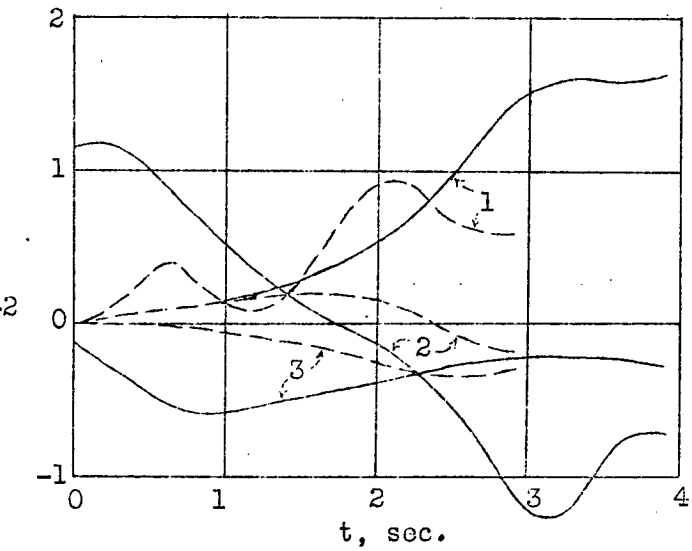

1, Gyroscopic moment
2, Static longitudinal moment.
3, Vertical damping.

Fig. 32 Decomposition of ω_ζ for case of Fig. 28 & 29.

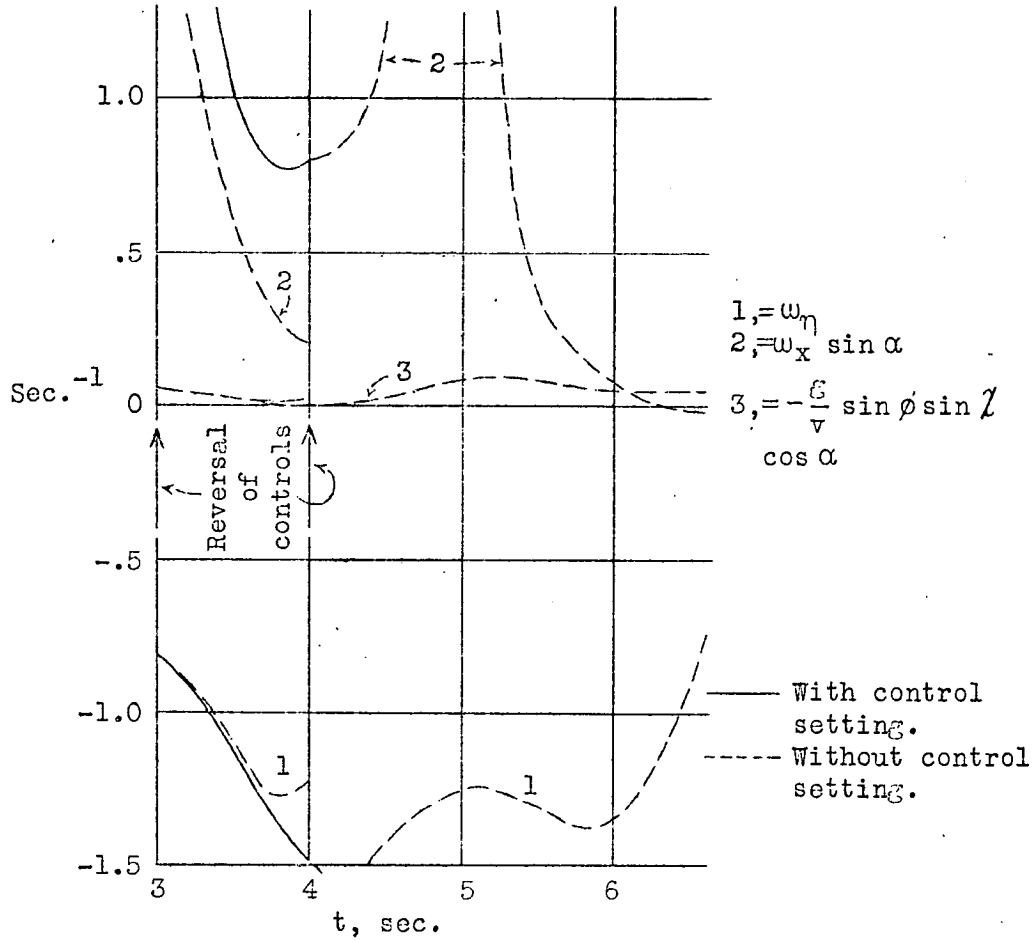

Fig. 33 Decomposition of τ during recovery from spin (Fig. 28)

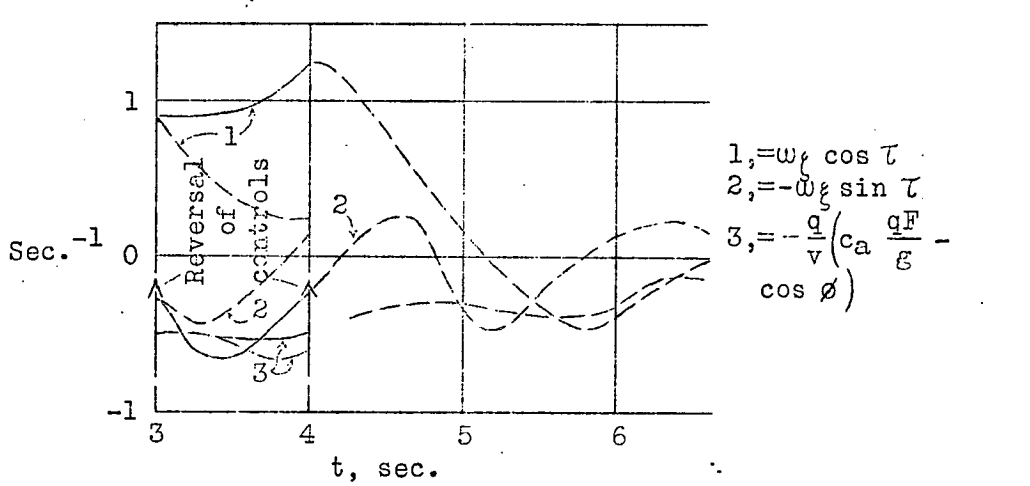

Fig. 34 Decomposition of α during recovery from spin (Fig. 28)

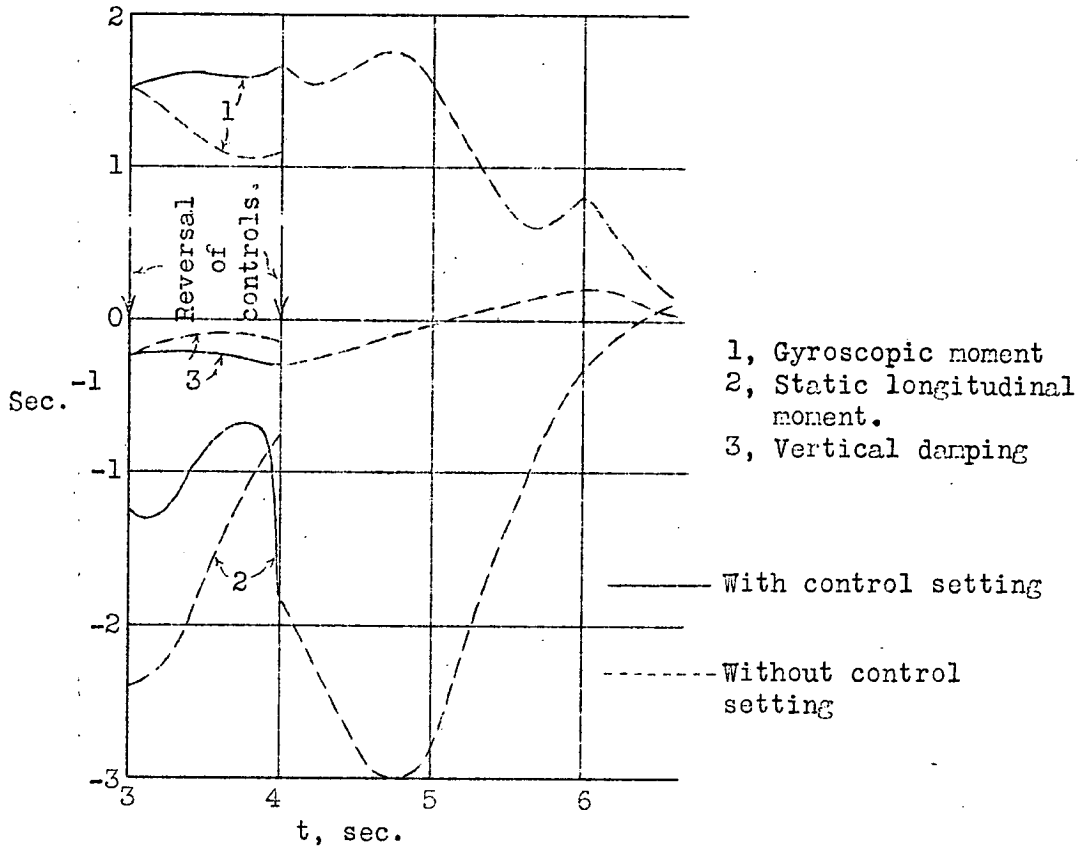

Fig. 35 Decomposition of ω_ζ during recovery from spin (Fig. 28)

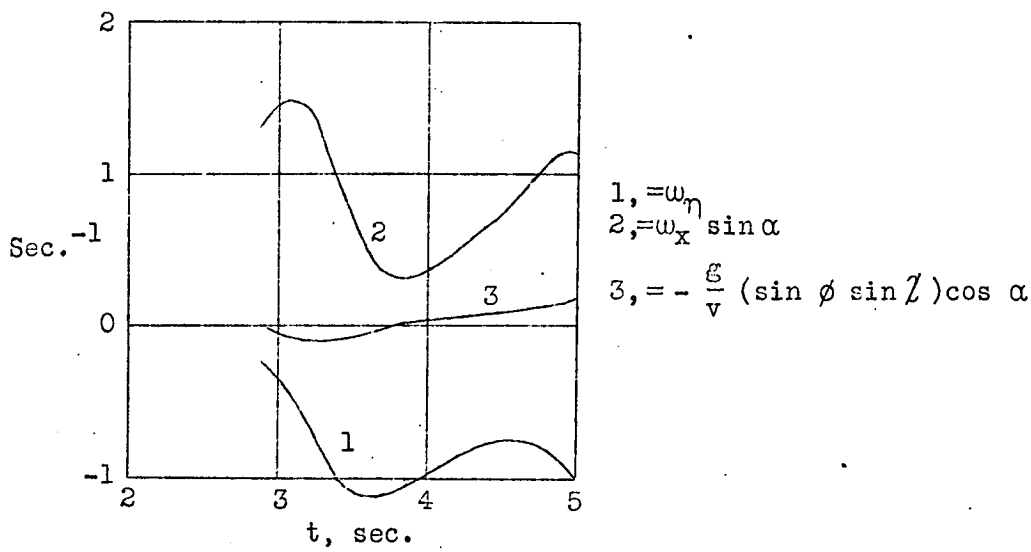

Fig. 36 Decomposition of τ during spin (Fig. 29)

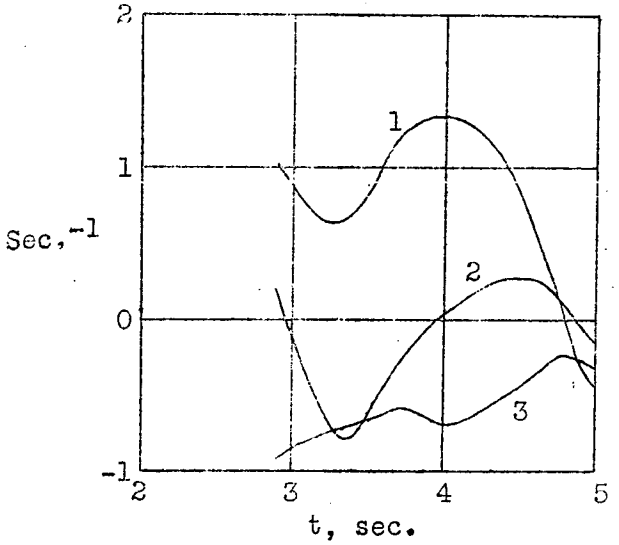

Fig. 37 Decomposition of α during spin (Fig. 29)

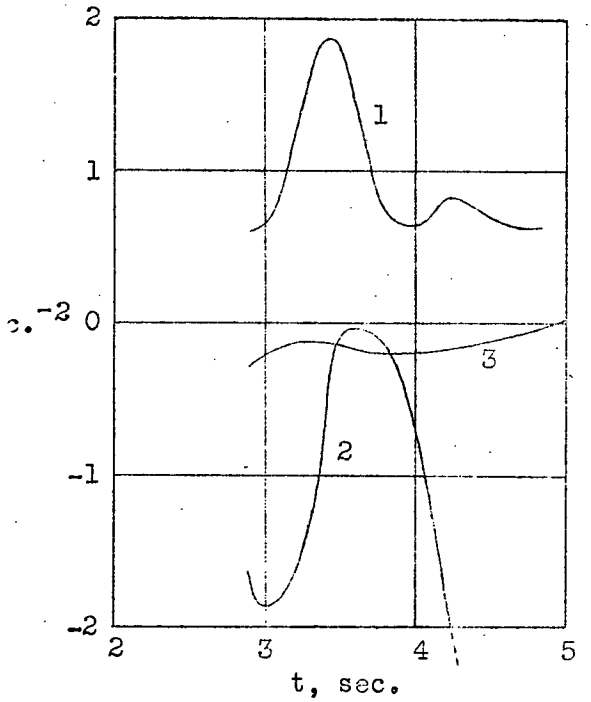

Fig. 38 Decomposition of ω_ζ during spin (Fig. 29)